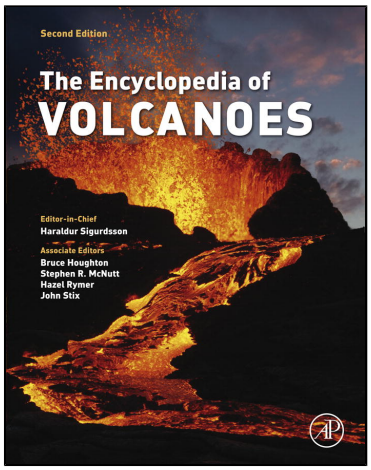

From Lesher, C.E., Spera, F.J., 2015. Thermodynamic and Transport Properties of Silicate Melts and Magma. In: Sigurdsson, H., Houghton, B., Rymer, H., Stix, J., McNutt, S. (Eds.), The Encyclopedia of Volcanoes, pp. 113–141.
ISBN: 9780123859389

Academic Press

Chapter 5

Thermodynamic and Transport Properties of Silicate Melts and Magma

Charles E. Lesher
Department of Earth and Planetary Sciences, University of California, Davis, CA, USA,
Department of Geoscience, Aarhus University, Aarhus, Denmark

Frank J. Spera
Department of Earth Science, University of California, Santa Barbara, CA, USA

Chapter Outline

Still, however, the highest value is set on glass that is nearly colorless or transparent, as nearly as possible resembling crystal. For drinking vessels glass has quite superseded the use of silver and gold

Pliny the Elder (c. AD 23–79)

GLOSSARY

basaltic magma Most typical type of magma erupted on Earth and other terrestrial planets. Basaltic magma is erupted at temperatures 1000–1300 °C, and is made up mainly of SiO_2 (50 wt%), Al_2O_3 (15%), CaO (12%), and roughly equal amounts of FeO and MgO (10%). The alkalis ($Na_2O + K_2O$) make up most of the difference although trace amounts of every naturally occurring element are invariably present. About 25 km^3 of basaltic magma is generated and erupted or emplaced each year on Earth, primarily along the 75,000 km of diverging plate boundaries. The density, specific heat, viscosity, and thermal conductivity of a typical basaltic magma at 1200 °C at low pressure are 2600 kg/m^3, 1450 J/kg K, 100 Pa s, and 0.6 W/m K, respectively. The heat needed to completely fuse (melt) gabbro, the plutonic (crystalline) equivalent of basaltic magma, is about 500 kJ/kg.

magma High-temperature multiphase mixture of solids (cognate crystals and exotic lithic fragments), silicate or carbonatitic liquid, and H–O–C–S–Cl-rich gas or supercritical fluid formed by partial or total melting of parental source material.

magma rheology The rheological properties of magma depend on temperature, bulk composition, pressure, phase assemblage (melt ± crystals ± vapor), particle size and shape distribution, spatial arrangement of particles (structure), and shear rate in a complex and intertwined manner characterized by multiple feedback loops.

magma transport phenomena This term encompasses all the dynamical processes responsible for the generation, ascent, eruption or emplacement of magma, its subsequent quenching or solidification, and interaction in hydrothermal magmatic systems. These processes involve simultaneous consideration of heat, mass, and momentum transport between relevant magmatic subsystems. Rates of momentum, heat, and mass transfer are widely varied ranging from creeping (percolative) flow of small degree partial melts through an otherwise solid parental source rock in response to pressure, buoyancy, and viscous forces to the rapid (several hundred meters per second) eruption of low density

The Encyclopedia of Volcanoes. http://dx.doi.org/10.1016/B978-0-12-385938-9.00005-5

The Encyclopedia of Volcanoes, Second Edition, 2015, 113–141

highly expanded magmatic mixtures characteristic of high-silica, volatile-rich rhyolitic magma that erupts to form pyroclastic flows of great natural hazard. The flow of magma in fractures, buoyant rise of magma diapirs and evolution of magma within crustal magma bodies that undergo simultaneous assimilation of wall rock, recharge of fresh parental magma and fractional crystallization and convective mixing (or unmixing) are all examples of magma transport phenomena.

metasomatism Metasomatism refers to the process whereby a pre-existing igneous, sedimentary, or metamorphic rock undergoes compositional and mineralogical transformations associated with chemical reactions triggered by the reaction of fluids (so-called metasomatic agents), which invade the protolith. A large-scale example is provided in subduction environments. Dehydration of hydrothermally altered oceanic crust and attached upper mantle generates fluids that migrate upwards and metasomatize the ultramafic mantle wedge lying above the subducting slab. Because the peridotite solidus temperature is lowered by the presence of water, metasomatism of the mantle wedge can trigger partial melting there. A smaller scale environment in which metasomatism is important occurs in contact metamorphic aureoles surrounding granitic plutons when emplaced into cooler preexisting crust. The magma body acts as a heat engine and drives hydrothermal circulation in the surrounding country rock. Economically important mineral deposits form in contact metamorphic environments.

rhyolitic magma Rhyolitic magma is erupted at temperatures 750−1000 °C, and is made up mainly of SiO_2 (75 wt%), Al_2O_3 (13%), and the Na_2O and K_2O in roughly equal amounts (3−5%). Only a small fraction of a cubic kilometer of rhyolitic magma is erupted each year mainly in continental environments although a significant fraction of rhyolitic and intermediate-composition magmas may stagnate at depth within the crust crystallizing there to form granitic plutons. Granitic batholiths are generally associated with subduction zone magmatism and can extend for hundreds to thousands of kilometers roughly parallel to the strike of oceanic trenches and along active continental margins. The density, specific heat, viscosity, and thermal conductivity of typical rhyolitic magma bearing 2 wt% dissolved H_2O at 900 °C at low pressure, are 2260 kg/m^3, 1450 J/kg K, 500,000 Pa s, and 1 W/m K, respectively. A water-free rhyolitic melt of otherwise identical composition has a density and viscosity of 2350 kg/m^3 and 1.2×10^{10} Pa s, respectively. The heat needed to completely fuse (melt) granite, the plutonic (crystalline) equivalent of rhyolitic magma, is ∼300 kJ/kg. Pristine volatile contents of typical rhyolitic magmas lie in the range 1−6 wt% and are mainly H_2O although finite amounts of CO_2 and sulfur-rich gasses (H_2S, SO_2, etc.) are also present. Volcanic gasses are often corrosive and contain HCl and HF as minor constituents.

thermodynamic properties Magma thermodynamic properties may be separated into two families: thermal functions and the equation of state (EOS). Thermal functions relate the temperature of a substance to its internal energy. These properties include the enthalpy, entropy, and heat capacity. The EOS relates the density of a substance to its composition, pressure, and temperature, and important properties include the isothermal compressibility and isobaric expansivity. The reactivity of a material depends on its chemical potential that involves both thermal functions and EOS data.

transport properties In typical dynamic (nonequilibrium) magmatic systems, gradients in pressure, stress or velocity, temperature, and chemical potential give rise to transport of momentum, heat, and mass, respectively. Momentum, heat, and mass can be transported by advective or diffusive flow. The transport properties that govern diffusive flow of momentum, heat, and mass are the viscosity, thermal conductivity and self, tracer and chemical diffusivities, respectively.

NOMENCLATURE

T Temperature (K)
P Pressure (Pa)
ρ Density (kg/m^3)
C_p Molar isobaric heat capacity (J/mol K)
c_p Specific isobaric heat capacity (J/kg K)
C_{pi}, c_{pi} Partial molar, specific isobaric heat capacity (J/mol K), (J/kg K)
S Entropy (J/K mol)
H Enthalpy (J/mol)
σ Interfacial surface energy (N/m)
β_T Isothermal compressibility,$(\partial \ln\rho/\partial P)_T$ (Pa^{-1})
α_P Isobaric expansivity, $-(\partial \ln\rho/\partial T)_P$ (K^{-1})
X_i Mole fraction of ith component
V_i Partial molar volume of ith component (m^3/mol)
K_T Isothermal bulk modulus (Pa)
K′ Pressure derivative of bulk modulus
η Viscosity (kg/m s ≡ Pa s)
E_A Activation energy for viscous flow (J/mol)
V_A Activation volume for viscous flow (m^3/mol)
η_r Relative viscosity, ratio of mixture viscosity to melt viscosity
ϕ Volume fraction dispersed phase (solid or vapor)
k_R Radiative (photon) conductivity (J/m K s)
k Thermal conductivity (J/m K s)
κ Thermal diffusivity, $k/\rho c_p$ (m^2/s)
D Self, tracer or chemical diffusivity (m^2/s)
E_a Activation energy for diffusion (J/mol)
V_a Activation volume for diffusion (J/mol)

Subscripts

fus fusion
form formation
conf configuration
mix mixing
r relative

1. INTRODUCTION

A central goal of studies in igneous petrology and volcanology is to understand the factors that lead to the compositional diversity of magmatic rocks and the related issue of the origin of the Earth's crust and mantle. In the crust are found essentially all of the material and energy resources accessible to the world population of 7 billion. This understanding is most powerful when framed in terms of

petrogenesis—the origin of **magma** and the rocks formed from cooling and solidification of magma—within the context of the coupling between the thermal evolution and chemical differentiation of Earth. The growth of oceanic and continental crust throughout the ~4560 million years of earth history, the extent of recycling of crust and lithosphere by subduction, the relationship of mantle plumes to the compositional differentiation of Earth, and the role of subduction in island arc magmatism and growth of continental crust are problems that studies of magmas and magmatic processes shed light upon. In addition, a close connection exists between magmatic diversity and practical problems, such as volcano forecasting, the mitigation of volcanic hazards, and the discovery of material and energy resources such as ore deposits and geothermal heat. The **thermodynamic** and **transport properties** of magma are central to all of these considerations.

There has been a sustained and accelerating effort in the last century to determine the properties of magma both in the laboratory and by application of models based on the chemistry and physics of materials. It is no exaggeration to claim that without these foundational measurements and theoretical models, petrology could not have evolved far beyond the purely descriptive stage. In this chapter, we provide an overview of current knowledge of the subject and future directions.

The composition of lava emitted from a volcanic center reflects both the composition of its source as well as myriad dynamical phenomena operating during its generation, segregation, ascent, residence time in crust (storage) and eruption. For the purposes of this chapter, magma is defined as a high temperature (generally >900 K), multiphase mixture of crystals, liquid, and vapor. The vapor can be either a gas or a supercritical fluid. Herein, the term liquid is used interchangeably with melt (i.e., they are synonyms) and fluid generally restricted to a phase that is rich in H, O, C, N, Cl, and S. The solid fraction of magma is primarily made up of oxide and silicate crystals, the relative abundance of which depends strongly on composition, temperature, pressure, and additional nonequilibrium or kinetic factors, such as cooling rate, rate of decompression, and rates of mass transfer by molecular diffusion, mechanical dispersion, and advective transport. Bits of local wall rock (lithic inclusions), cognate crystal cumulates, or exotic xenoliths are also commonly found in plutonic and volcanic rocks and provide clues to understanding magma genesis and dynamics as well as a providing constraints on the bulk composition of the source. The liquid or melt portion of magma is generally a multicomponent (O−Si−Al−Ca−Mg−Fe−K−Na−H−C) silicate liquid; crustal melts (silicic or rhyolitic to intermediate or andesitic) are rich in O−Si−Al−Na−K−H whereas melts generated within the Earth's mantle are richer in O−Si−Al−Ca−Mg−Fe (mafic or basaltic). Carbonatitic melts containing >50 wt% carbonate are also generated within the mantle. Although the volumetric rate of eruption of carbonatitic magma is very small compared to the roughly 25 km^3/year of mid-ocean ridge basaltic magma produced, rare carbonatitic magmas may be important agents for mantle **metasomatism**. Carbonatites also have an affinity with economically important diamond-bearing kimberlitic magmas, which are rapidly erupted from depths of several hundred kilometers, if not more.

Common magmas vary nearly continuously in composition from basaltic (50 wt% SiO_2) to rhyolitic (75 wt% SiO_2). These magmas usually contain small amounts (on the order of a few weight percent) of dissolved H_2O, CO_2, and other volatile species such as H_2S, N_2, HCl, HF, COS, and SO_2. H_2O dissolved in melts occurs in two forms: molecular H_2O and as the hydroxyl polyanion OH^-. The ratio of molecular water to hydroxyl depends on the composition (devolatilized) of the melt. When sufficient volatile components are present, melt becomes supersaturated and a discrete vapor or supercritical fluid forms. This fluid has a low viscosity and density compared to silicate melts and is particularly rich in the components O−H−C−S−N−Cl−F. The speciation of this fluid depends on bulk composition, temperature, and pressure. At crustal pressures and temperatures, supercritical fluids, especially those rich in molecular H_2O, are quite corrosive and can dissolve a few percent or more by mass of other oxide components. In part, this is due to H_2O's dipolar nature and large dielectric constant making it a good solvent. At very high pressure and temperature even larger quantities of solid may dissolve in these fluids, while at conditions of subduction zone magmatism, i.e., depths of ~100 km (3 GPa) and temperatures of 700−1400 °C, silicate melt and hydrous fluids can be completely miscible. The concentration of dissolved volatiles in a melt is strongly dependent on pressure because the partial molar volume of a volatile species in the dissolved state is much smaller than its molar volume in the gaseous or supercritical fluid state. It is this difference in volume that relates the Gibbs free energy, and hence solubility, to pressure at fixed temperature. The huge volumetric expansion of a magmatic mixture that accompanies exsolution of volatiles is one of the primary causes of explosive volcanism as pressure−volume (PV) expansion work is converted to kinetic energy. Although at depths of a few kilometers magma ascent rates may be only a fraction of a meter per second, once volatile exsolution commences and PV work is converted into kinetic energy, magma eruption speeds of order 100−300 m/s can easily develop. Other factors, such as magma viscosity and the rates of volatile component diffusion, and their variations with temperature and pressure are also important in assessing the dynamics of explosive volcanism.

TABLE 5.1 Estimated Properties of Common Natural Melts at 1 bar (10^{-4} GPa) at Their Respective Liquidus Temperatures. All Compositions Are Anhydrous Except Where Indicated. See Tables S5.1–S5.7 for More Exhaustive Compilations of These Properties.

Composition	Liquidus Temperature (°C)	Specific Heat of Fusion (kJ/kg) Δh_{fus}	Density (kg/m^3) ρ	Specific Isobaric Heat Capacity (J/kg K) c_p	Melt Viscosity (Pa s) η
Granite (dry)	900	220	2349	1375	1.2×10^{10}
Granite (2 wt% H_2O)	900	250	2262	1604	5×10^5
Granodiorite	1100	354	2344	1388	1.3×10^6
Gabbro	1200	396	2591	1484	30.0
Eclogite	1200	570	2591	1484	–
Komatiite	1500	540	2748	1658	0.15
Peridotite	1600	580	2689	1793	0.25

Volcanic rocks, in particular, play a unique role in efforts to understand magmatic transport phenomena because, unlike plutonic rocks, they are quenched relatively rapidly and provide more or less direct information regarding the composition of natural melts. In order to understand the significance of the chemical composition of volcanic rocks, the dynamical and physical aspects of its parental magma evolution must first be unraveled. This is not an easy task. The range of transport phenomena of potential relevance to petrogenesis is quite varied and covers large spatiotemporal scales. Although the dynamics can be complex, it is clear that the thermodynamic and transport properties of magma are absolutely pivotal to the success of any quantitative dynamical theory of magma genesis and transport. If twentieth-century research in petrology can be summarized in a few words, it was the century of quantification—quantification of the energetics of magma. Although far more needs to be learned, it is reasonable to claim that geologists now have a first-order understanding of the basic properties of the common magma types and are beginning to understand how such properties relate to igneous petrogenesis—the origin of igneous rocks. In the twenty-first century, new instrumental techniques are providing a treasure trove of information regarding the composition of crystals, glass inclusions, and grain boundaries at the micron- to nanoscale. This information must ultimately be connected to dynamics of magmatic systems through the macroscopic petrogenetic prism. This will require an even better understanding of the properties of melts and magmas. In this chapter, the most critical properties will be briefly reviewed in the context of petrogenesis. Representative data are presented in the figures, Tables 5.1 and 5.2, and 11 data compilations archived as Supplementary Material Tables S5.1– S5.11. These compilations are not exhaustive and particular research applications may require a return to the original sources for additional details. Some of these sources are listed in Further Reading and many more are provided in the Supplementary Material section. The Nomenclature includes symbols used in the text.

2. MAGMATIC SYSTEMS: TIME AND LENGTH SCALES

Lifetimes of magmatic systems and processes vary widely—from the rapid radiative quenching of a millimeter-sized melt droplet (pyroclast) during its high-speed ejection from a vent (several seconds), to the slow cooling of a single lava flow (weeks or months), to the hundred thousand to million-year timescale of a large pluton cooling mainly by phonon (heat) conduction and hydrothermal convection. Individual magmatic hydrothermal systems, such as at Yellowstone National Park, USA, can remain active for a few millions of years because heat conduction is intrinsically a slow process (rocks are good insulators) and because many magmatic systems are open systems replenished by entry of magma rising from deeper in the crust or mantle below. This replenishment or recharge magma is often hotter than resident magma because it comes from greater depths where higher temperatures are usually found. In terms of dynamical process, creeping percolation flow in a partial melt region is of the order of several meters or less per year and may be contrasted with the explosive eruption of a volatile-rich magma at several hundred meters per second. Although rates of heat, mass, and momentum transfer are wildly different in these systems or subsystems, knowledge regarding the

TABLE 5.2 Representative Phonon Thermal Conductivity of Geosilicate Liquids and Glasses, and Olivine. Data Sources and More Exhaustive Data Compilations Are Provided in Tables S5.8 and S5.9. Experimental Measurements Are Given in Roman Type. Values in Italic Type Are Determined From Recent MD Simulations (Tikunoff and Spera, 2014).

Composition	Temperature (°C), Pressure (GPa)[1]	Thermal Conductivity (W/m K)
Olivine (Fo_{90})	800	2.69
	1400	2.18
Olivine (Fo_{100})	1400	1.59
Basalt (glass)	300	1.48
Obsidian (rhyolite glass)	300	1.67
Rhyolite (liquid)	800–1100	1.5
$NaAlSi_3O_8$ (glass)	800	1.56
$NaAlSi_3O_8$ (liquid)	1200	1.59
	1800	*1.45*
	1800, 10	*2.16*
$CaMgSi_2O_6$ (glass)	800	1.46
$CaMgSi_2O_6$ (liquid)	1100	1.21
	1800	*1.14*
	1800, 10	*2.02*
Mg_2SiO_4 (liquid)	3000	*1.06*
	3300	*0.90*
	3300, 10	*2.11*

[1]*Pressure is 1 bar (10^{-4} GPa) unless noted.*

thermodynamic and transport properties of magma is critical in order to meaningfully analyze and ultimately predict the relevant dynamics regardless of the particular scale.

Length scales relevant to magma transport and genesis also vary over many orders of magnitude. At the smallest scale, submicrons to millimeters, nucleation and growth of crystals, or vapor bubbles depend on local fluctuations in melt structure and the rates of mass diffusion. At larger scale, differentiation involves the physical separation of crystals, melt, and vapor in conduits and chambers over meters to kilometers, while the generation, transport, and ponding of magmas can extend over hundreds of kilometers. Batholithic terrains, the product of multiple emplacement of many individual plutons have aerial extents on the order of thousands of square kilometers. In the early part of Earth history, a globe-encircling magma ocean hundreds to thousands of kilometers deep may have existed. Modeling this system demands knowledge of the properties of magma and phase equilibria for temperatures in the range 1000–5000 K and pressures at the Earth's surface (10^{-4} GPa = 1 bar) to the core–mantle boundary (135 GPa). Thus, knowledge of the physical properties of magmas is essential to virtually all facets of magmatism throughout Earth history at a wide variety of scales in space and time, including the environmental impacts and hazards of volcanism on virtually all inhabitants of our planet. This is the realm of Earth System Petrology. Because the terrestrial planets and minor bodies (asteroids) of the solar system have a similar origin, study of magmatism is also a key element in understanding solar system origin and early evolution. It has been estimated that tens of billions of terrestrial planets, that is, planets composed of metal and rock, exist in the Milky Way galaxy, one of about 300 billion galaxies in the observable Universe. The properties of high-temperature silicate melts and magmas are therefore relevant to phenomena at cosmological scales throughout the past 13.8 billion years.

3. MAGMA THERMODYNAMIC PROPERTIES

Magma properties can be separated into two groups—equilibrium thermodynamic quantities and transport properties. Important equilibrium thermodynamic quantities include density (ρ), heat capacity (C_P), third law and configurational entropies (S), enthalpies of formation (ΔH_{form}), fusion (ΔH_{fus}), mixing (H_{mix}), and interfacial surface energy (σ). Application of equilibrium thermodynamic data are most useful in addressing the influence of source bulk composition, pressure, and temperature on the composition and amount of melt generated during partial fusion, as well as the composition of solids and residual melts during solidification of magma. Although chemical and thermal equilibrium are not perfectly attained in nature, the concept of local equilibrium is useful because equilibrium is often closely approximated at some scale and because it represents a reference state from which deviations from equilibrium can be assessed. When chemical equilibrium is assumed, all the classical theory of chemical thermodynamics can be applied and many times this greatly simplifies a problem and allows one to test and discriminate between competing hypotheses. For example, at constant temperature and pressure, minimization of the Gibbs free energy for a fixed bulk composition allows one to compute the composition and abundance of each phase in the equilibrium assemblage. To compute the energetics of melting, heat capacities and enthalpies of fusion of appropriate phases are essential. Although not strictly an equilibrium process, calculation of magma heat transport

requires heat capacity and fusion enthalpy data, in addition to thermal diffusivities. The variation of melt density with temperature, pressure, and composition is needed for analysis of momentum transport since buoyancy is a significant factor driving the segregation, ascent, and eruption of magma. The differentiation of an emplaced magma body by gravity-driven crystal fractionation critically depends on the density difference between melt and newly formed crystals. Like an iceberg in the ocean, there are conditions in temperature and pressure space where crystals grown in a melt float rather than sink. The final solidified state of such a system is obviously quite dependent upon the equation of state (EOS)—the relationship between density, temperature, and pressure—for all relevant phases. For example, the compressibility of magma, defined according to $\beta_T = (\partial \ln\rho/\partial P)_T$, informs us about the variation of magma density with pressure and is therefore important for constraining buoyancy force(s) driving magma ascent and the depths of ponding where the density contrast between magma and host rock vanishes. Magma compressibility also is an important factor governing the explosivity of magma at or near the earth's surface, especially for degassing, volatile-rich magmas. These examples show that there is a deep connection between the equilibrium thermodynamic properties of magma and its petrogenetic transport history. Without fundamental property data, it is impossible to exploit the equations governing conservation of energy, mass, species, and momentum to solve quantitatively magma transport problems. The equilibrium chemical thermodynamic model provides a logical starting point for the analysis of magma production.

Natural silicate melts contain SiO_2, Al_2O_3, MgO, CaO, iron oxides, the alkalis (Na_2O and K_2O), P_2O_5, transition metals, and rare earth elements, and minor but important amounts of volatile compounds made up of H−O−C−S−Cl−F−N. A complete thermodynamic description of such a complex multicomponent system over the relevant range in temperature−pressure−composition space is beyond the scope of this chapter (see Chapter 6—Chemical Thermodynamics and the Study of Magmas by M. Ghiorso and G. Gualda—for details). Many excellent reviews have also been published on the thermodynamic properties of silicate liquids including the relationship between structure and properties listed. A few of these are listed in Further Reading. We summarize the salient features here.

3.1. Density and EOS

The density of a silicate melt may be determined by evaluating the quotient

$$\rho = \Sigma X_i M_i / \Sigma X_i V_i \qquad (5.1)$$

where X_i is the mole fraction, M_i is the molar mass, and V_i is the partial molar volume of the ith oxide component in the melt. Although V_i depends weakly on composition, to a good approximation, it may be taken independent of composition and as a function of temperature and pressure for most petrological calculations. Partial molar isothermal compressibilities for the major oxide components have been determined from ultrasonic sound speed laboratory experiments. These parameters can be used to compute melt density as a function of temperature, composition, and pressure up to several GPa using a simple empirical EOS

$$V(T,P,X) = \sum X_i \left[V_{i,T_r} + \left(\frac{\partial \overline{V_i}}{\partial T}\right)_P (T - T_r) + \left(\frac{\partial \overline{V_i}}{\partial P}\right)_T (P - P_r) \right] \qquad (5.2)$$

where T_r and P_r are reference conditions (generally 1400 °C and 10^{-4} GPa (1 bar), respectively) and V_i is the partial molar volume of the ith component. Parameters for computing melt density as a function of pressure (up to several GPa) and temperature is presented in Table S5.1. Densities of some common natural melts at their respective approximate liquid temperatures are given in Table 5.1 (and Table S5.2) and shown graphically as a function of temperature and volatile content in Figures 5.1 and 5.2. As a rule of thumb, adding FeO, Fe_2O_3, MgO, TiO_2, and CaO to a melt increases its density, whereas adding alkalis (Li_2O, Na_2O, and K_2O) and volatiles (H_2O, CO_2) have the opposite effect. The temperature derivative of the partial molar volumes of SiO_2 and Al_2O_3, are both effectively zero. As a

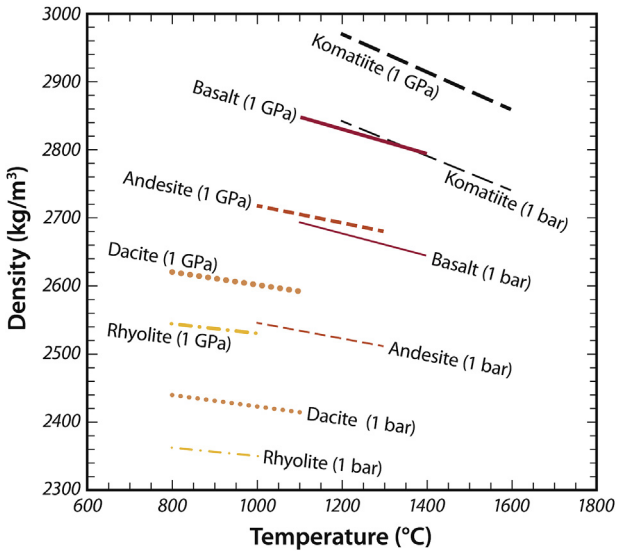

FIGURE 5.1 Melt density as a function of temperature for natural melts spanning the compositional range rhyolite to komatiite at 1 bar (10^{-4} GPa) and 1 GPa pressure. All compositions are volatile-free.

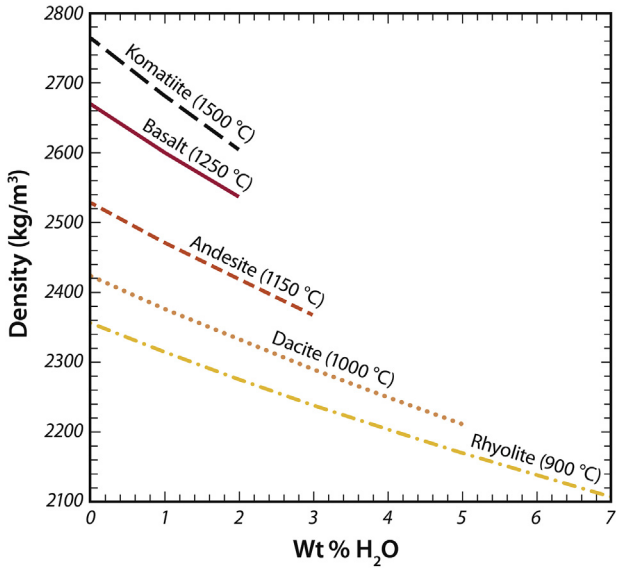

FIGURE 5.2 Melt density as a function of dissolved water content for natural melts spanning the range rhyolite to komatiite. Temperatures for each composition are characteristic eruption temperatures. Densities are calculated at a pressure of 1 bar (10^{-4} GPa).

consequence, the density of a melt rich in silica and alumina is quite insensitive to temperature. Densities of melts vary from 2500 to 2900 kg/m^3 at magmatic temperatures (~1100 °C) for silicic through intermediate to mafic and ultramafic compositions at low pressure. Density increases as pressure rises, although increasing the concentration of the alkaline earth metals, Ca, and Mg, serves to decrease the pressure dependence of melt density. The alkali metals and water are relatively compressible and contribute significantly to the pressure dependence of density. It is important to note that small differences in composition can compensate for relatively large differences in temperature because of the strong dependence of melt density on composition. Whereas a typical value for the isobaric expansivity is $\alpha_P = -(\partial \ln \rho/\partial T)_P \approx 5 \times 10^{-5}$/K, the analogous quantity describing the variation of density with composition is of order 0.1 to 3 depending on the component. The volatile components H_2O and CO_2 have an especially large effect on melt density. The partial specific density (M_i/V_i) for CO_2 and H_2O in natural melts are ~1400 and 900 kg/m^3, respectively, for typical crustal magmas. For comparison, M_i/V_i for K_2O, MgO, FeO, and SiO_2 are ~2000, 3500, 5300, and 2200 kg/m^3, respectively. Thus, a small amount of dissolved water dramatically lowers melt density and significantly affects transport and thermodynamic melt properties such as viscosity, mass diffusivities, thermal conductivity, and isobaric heat capacity. The temperature at which rocks begin to melt (the solidus temperature) is substantially lowered when volatile constituents such as H_2O are present. Because oxygen is volumetrically by far the most abundant anion in the silicate Earth, the major incorporation mechanism of H_2O into nominally anhydrous silicates and oxides, including melts, is as the hydroxyl anion, OH^-. Almost all of the nominally anhydrous minerals that compose the earth's crust and mantle can incorporate measurable amounts of "water." The amount of water (generally as OH^-) incorporated into nominally anhydrous minerals generally increases with pressure and sometimes with temperature, and is typically in the range 50–300 ppm in the dominant minerals of the earth's upper most mantle (olivine, pyroxenes, and garnet). The solubility of water in the $(Mg,Fe)_2SiO_4$ polymorphs wadsleyite and ringwoodite stable in the transition zone (~410 to ~660-km-depth) is markedly higher, and in total it has been estimated that several ocean's worth of water may be present in Earth's mantle. The recent discovery of upward of 1 wt% water in ringwoodite encapsulated in a natural diamond from a Brazilian kimberlite bolsters the claim that much of the water recycled into the deep mantle is trapped by the transition zone. This has important implications for the phase relations, dynamics, and magmas formed by partial melting of the mantle.

The change in volume of a crystalline silicate upon fusion under isobaric conditions is important because it influences the slope of the melting curve in pressure–temperature space and therefore the generation of magma by partial fusion. For small degrees of partial melting under nearly isochoric conditions, melt pressure can rise above lithostatic values and the small melt overpressure can drive magma fracture and vertical transport. Additionally, melt density influences the separation rate of melt from its source. Volume changes accompanying melting of some silicates are given in Table S5.2. Typically, the molar volume of a crystalline phase increases by about 10% upon fusion although silica (like ice) may shrink (i.e., become more dense) when fused at low pressure. Less is known regarding density–temperature–pressure relations or EOS for natural carbonatite melts. Some data pertaining to the density and viscosity of simple carbonate liquids as well as supercritical H_2O are given in Table S5.3. Relative to common silicate melts, carbonatite liquids are both less dense (by about 30%) and less viscous by several orders of magnitude compared to mafic melts and up to 10 orders of magnitude compared to silicic ones.

At pressures corresponding to depths greater than about 100 km (>3 GPa), the density of melts at superliquidus temperatures can be determined from high-pressure static (sink–float) and shock wave experiments. More recently, a vast array of spectroscopic tools, including X-ray absorption, tomography and diffraction/scattering, and ultrasonic measurements in conjunction with static high-pressure conditions are being employed to augment data obtained by more traditional approaches—in some cases accessing subliquidus conditions more directly applicable to magma

genesis and differentiation. First-principles or classical molecular dynamics (MD) simulations are increasingly being utilized as a complement to experimental measurements, and enable predictions beyond experimental reach.

A useful quasi-theoretical relationship is the Birch–Murnaghan EOS that relates liquid (of fixed composition) density to pressure and temperature according to:

$$P = \frac{3}{2}K_T\left[\left(\rho/\rho_{T,0}\right)^{7/3} - \left(\rho/\rho_{T,0}\right)^{5/3}\right]\left[1 - \frac{3}{4}(4 - K')\left(\rho/\rho_{T,0}\right)^{2/3} - 1\right] \quad (5.3)$$

where $\rho_{T,0}$ is the density of melt at 10^{-4} GPa and temperature T, K_T is the isothermal bulk modulus ($K_T = 1/\beta_T$) at 1 bar (10^{-4} GPa), K' is the pressure derivative of K_T, and ρ is the melt density at pressure P and temperature T. Many other equations of state have been proposed and find application in geoliquids. Compressibility data for silicate melts are presented in Table S5.4. Normalized density–pressure relations for silicate liquids ranging from felsic to ultramafic compositions are shown in Figure 5.3. Polymerized rhyolite liquid possessing an open network structure is vastly more compressibility than basalt or andesite, while highly depolymerized and compact melts such as komatiite and peridotite are the least compressible. An interesting application of high-pressure EOS studies is that MgO-rich komatiitic melts, probably the most common magma type erupted in the first billion or so years of earth history, become denser than olivine crystals at pressure corresponding to depths of roughly 250–400 km. This has important implications for differentiation of the silicate portion of Earth including internal mineralogical layering as well as possible chemical stratification. Moreover, the compressibility of silicate liquids also bears on the dynamic stability of melts in the mantle, and the interpretation of low seismic velocity regions there. Models calling on the presence of (neutrally buoyant) melt immediately above the core–mantle boundary (ultra low-velocity zone), at the top of the transition zone (~410 km), and at a depth of about 220 ± 30 km (Lehmann discontinuity) depend critically on the details of how silicate melts densify as pressure increases. This is an area of very active research.

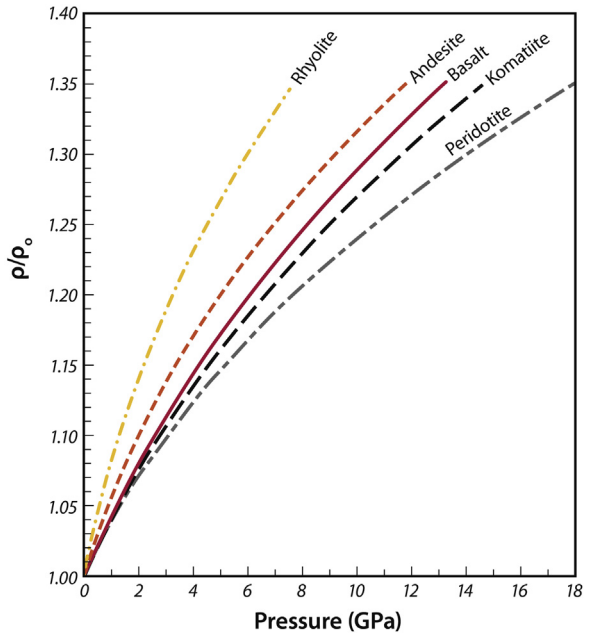

FIGURE 5.3 Normalized density (ρ/ρ_o) at 2000 K as a function of pressure for natural silicate liquids ranging in composition from rhyolite to peridotite computed using Eqn (5.3) and parameters from Table S5.4, assuming an average $dK_T/dT = -0.022$.

3.2. Enthalpy, Entropy, and Heat Capacity

In addition to volumetric or EOS data, the calorimetric properties of high temperature and molten silicates are needed to analyze magma transport problems. These properties inform us regarding the internal energy of melts and crystals and how internal energy and other closely related thermodynamic functions change with temperature. These properties include the enthalpy, entropy, and heat capacity and are inextricably bound to the thermal evolution of magma and relevant to processes such as partial melting, solidification, and the advective transport of heat. Melting temperatures, enthalpies of fusion, entropies of fusion, and specific heats of fusion for some common phases are listed in Table S5.5. The specific enthalpy of fusion is the heat per unit mass needed at a reference pressure (generally 10^{-4} GPa or 1 bar) to transform a crystal or crystalline assemblage to the liquid state. There is a wide variation in the specific enthalpy of fusion from 100 to 300 kJ/kg for silica polymorphs, albite, and sanidine, all important components in crustal-derived melts, to ~1000 kJ/kg for refractory phases, such as forsterite, pyrope, enstatite, and transition metal oxides relevant to mafic and ultramafic compositions. Table 5.1 provides estimates of fusion enthalpies for common compositions computed using data from Table S5.5 and typical modal abundances. There is a factor of three difference in the specific heat of fusion for a model granite (~200 kJ/kg) compared to an ultramafic composition (~600 kJ/kg). The more refractory nature of the ultramafic composition is a reflection of the higher fusion enthalpy of olivine and the pyroxenes relative to quartz, alkali feldspar, and plagioclase. Garnet also has a high specific fusion enthalpy. Melting eclogite (pyroxene plus garnet) at high pressure requires more heat (570 kJ/kg) than a corresponding low-pressure plagioclase-pyroxene gabbro (~400 kJ/kg). The relatively low fusion enthalpy for mineral phases comprising continental crust implies

that anatexis of crust by heat exchange between mafic magma and its surroundings is thermally efficient. It is worth noting that the heat required to completely melt Earth's mantle $\sim 3 \times 10^{30}$ J, is less than 10% of the kinetic energy delivered to Earth by impact of a Mars-sized body (15% mass of Earth) with an impact velocity equal to the Earth's escape velocity of 11.2 km/s. If, in fact, the earth did possess a magma ocean in the Hadean, then its lifetime would have been controlled by the rate at which $\sim 10^{30}$ J of heat could be dissipated by conduction, radiation, and convection to space.

In addition to heat effects associated with solid to liquid phase changes, it is important to consider sensible heat effects or the variation of the enthalpy of the melt with temperature. This is measured by the molar isobaric heat capacity, C_p. For most aluminosilicate glasses and melts of petrologic significance, C_p can be approximated as an additive function of oxide component partial molar isobaric heat capacities. As temperature increases for glasses, an increased number of vibrational modes become excited and so the isochoric heat capacity $C_V \equiv (\frac{\partial E}{\partial T})_V$ increases toward the high temperature Dulong–Petit limit as vibrational modes become saturated. The isobaric heat capacity is related to the isochoric one by the expression $C_P = C_V + \frac{T\alpha_T^2}{\rho\beta_P}$. Parameters for the common oxide components to estimate the isobaric heat capacity of a glass as a function of composition and temperature at low pressure are listed in Table S5.6. At the glass transition temperature (T_g), there is generally a discontinuous jump in isobaric heat capacity. The magnitude of this jump depends on the atomic structure of the liquid. Highly polymerized melts—so-called, strong liquids—exhibit little or no discontinuity in heat capacity at T_g, while depolymerized, i.e., fragile, melts do. For petrologic purposes, it is sufficient to note that the jump in C_p at the glass transition temperature is small for silica-rich liquids (e.g., rhyolitic melts) and it becomes larger for more mafic liquids (andesitic and basaltic melts).

For silicate melts (unlike silicate glasses), the temperature dependence of C_p can generally be neglected unless great accuracy is required. Parameters for estimating C_p for melts as a function of composition at magmatic temperatures are presented in Table S5.7. Table 5.1 gives specific isobaric heat capacities (c_p) for some common naturally occurring anhydrous silicate melts. Silicic anhydrous melts have c_p around 1300–1400 J/kg K, whereas melts with higher MgO contents have specific heats around 1600–1700 J/kg K. Because the advective transport of heat per unit volume is given by $\rho c_p \Delta T$ magmas are good transporters of mantle heat to crustal levels since ΔT is of order 100–1000 K. Magmatic water content can also have a large effect on the heat capacity of magmas. The partial isobaric heat capacity of water dissolved as hydroxyl $(OH)^{-1}$ is $\sim$13,000 J/kg K, while water dissolved in its molecular form (H_2O) has a partial isobaric heat capacity of $\sim$4700 J/kg K. For comparison, c_p for ambient tap water is 4184 J/kg K. Likewise, the isobaric heat capacity of silica glass increases by $\sim$30% with the addition of 1200 ppm OH, while adding 2 wt% H_2O to an otherwise anhydrous granitic melt will increase c_p by 20%. Thus, the addition or loss of magmatic volatiles (namely water) can have significant enthalpic effects that, in turn, will influence ascent rates, eruptibility, solidification timescales, and countless other magmatic processes.

4. MAGMA TRANSPORT PROPERTIES

Transport properties of magma play a crucial role in development of petrogenetic theory. Simple consideration of the various stages of magma transport from source to surface makes this abundantly clear. Some examples include the generation of magma by partial melting, melt segregation by porous or channel flow, and magma ascent by viscous flow in magma-filled propagating cracks. Other examples include differentiation of magma by crystal fractionation and the processes of magma mixing and crustal anatexis. In all these phenomena, significant amounts of momentum, heat, and chemical component transport occur. Transport of momentum, heat, and chemical species by magmas involves the material properties of viscosity, thermal conductivity, and mass diffusivity, respectively. Although data and models for the composition and temperature dependence of melt viscosity are available, less is known regarding the quantitative rheological properties of magmatic mixtures. There are relatively few experimental data bearing on the thermal conductivity of melts at high temperatures; this is perhaps the most uncertain of all magma transport properties but one with significance with respect to the thermal history of the Earth. Chemical, self, and tracer diffusivity data exist and correlations have been developed for estimating diffusivities as a function of species charge and size for melts of various temperature and composition, and treating more complicated multicomponent diffusion and associated isotopic effects. The effects of pressure are not well understood, but systematics are emerging for network former and network-modifying cations exhibiting different pressure dependencies. A brief review of these properties is presented below. The original references should be consulted for more detail.

4.1. Melt Viscosity

The dynamic viscosity (η) of magma is the material property that connects the shear stress in the fluid to the rate of strain. The viscosity determines the rate of diffusion of

momentum. More precisely, the kinematic viscosity, defined $\nu = \frac{\eta}{\rho}$, measures the tendency of a melt or magma to diffuse velocity gradients. Critical issues include the effect of composition, pressure, and temperature on melt viscosity, as well as the rheological properties of magmatic suspensions. Although to a good approximation silicate liquids well above the glass transition temperature behave as Newtonian fluids (that is, they show a linear relationship between shear rate and shear stress at fixed temperature and pressure), this is not the case for magmatic multiphase suspensions that generally exhibit complex rheological properties or for natural glasses that are described as viscoelastic materials.

The temperature dependence of melt viscosity can be described by several models. The simplest is the Arrhenian model for a melt of fixed composition

$$\eta(p,T) = \eta_o \exp[(E_A + PV_A)/RT] \qquad (5.4)$$

In expression (5.4), η_o is the asymptotic viscosity as $T \to \infty$, E_A is the activation energy for viscous flow, V_A is the activation volume for viscous flow, and R is the universal gas constant. The activation energy and volume are constants for melt of fixed composition. The preexponential term is approximately a "universal" constant that varies quite weakly with composition and is in the range 10^{-4} to 10^{-5} Pa s. An optimal value of $\eta \approx 10^{-4.6}$ Pa is found empirically for melts in the range of natural compositions. Activation energies vary systematically with composition from values around 200 kJ/mol for mafic and ultramafic melts to 400 kJ/mol for more silicic compositions. Increasing the concentration of nonframework components such as the alkalis, the alkaline earths, and especially H_2O results in creation of oxygens with only a single nearest neighbor of Si or Al. The presence of these nonbridging oxygens (NBOs) destroys the network structure created by the linkage of tetrahedra to form 3 to 6+ membered rings at intermediate atomic scales of order 0.5–1 nm. For the ideal network tetrahedral melt, each oxygen is bound to two Si, two Al or one Si, and one Al simultaneously. The archetypal example is molten silica in which each oxygen has two nearest neighbors of silicon and each silicon is surrounded by four nearest neighbors of oxygen. The increase in the concentration of NBO by addition of network modifiers (e.g., H_2O) lowers E_A. Small (several percent by mass) concentrations of water have a dramatic effect in lowering the viscosity of silicate liquids because water is 89% oxygen (by mass) unlike any other common oxide component. This is illustrated in Table 5.1 for the granitic composition where the addition of 2 wt% H_2O to a granitic melt lowers melt viscosity by a factor of 10^5. H_2O also tends to lower the viscosity of more mafic compositions, although the effect is less dramatic because fewer bridging oxygen (BO) exist in anhydrous mafic melts.

The relationship between liquid structure at the atomic level and macroscopic properties (both transport and thermodynamic) is an essential keystone of **magma transport phenomena**. The activation volume, a measure of the pressure dependence of viscosity, is usually a small fraction of the molar volume of the melt and changes sign, from negative to positive, as the fraction of NBO increases and in the case of polymerized melts pressure increases. A typical value for V_A for a network tetrahedral melt such as $NaAlSi_3O_8$ at low pressure is around -6×10^{-6} m^3/mol (-6 cm^3/mol), whereas for more depolymerized melt (e.g., $CaMgSi_2O_8$) V_A is around 3×10^{-6} m^3/mol ($+3$ cm^3/mol). Melts with a negative value of V_A show a decrease in viscosity as pressure increases—the opposite is true for melts with positive V_A.

Fully polymerized network melts, for which essentially all the oxygen is BO typically possess intermediate range order defined by the formation of n-membered rings ($n = 4$–10) of tetrahedra at low pressure. As pressure increases, the ring structure collapses and the "anomalous" effect of viscosity ($-V_A$) diminishes to a point that free-volume effects dominate and viscosity increases with pressure ($+V_A$). Elevated pressure also drives oxygen into higher (five and sixfold) coordination with Si and Al and such changes in the network structure also have been linked the change from anomalous to normal pressure dependence of viscosity.

Not all silicate melts follow the Arrhenian temperature–viscosity relationship. This is especially true for fragile liquids, e.g., melts containing a high proportion of NBO. An empirical relationship for predicting the temperature dependence of viscosity data in fragile non-Arrhenian melts at 1-bar pressure is the so-called Tammann–Vogel–Fulcher (TVF) expression

$$\eta = \eta_O \exp[B/(T - T_K)] \qquad (5.5)$$

where B and T_K are functions of composition but not temperature. T_K is a constant closely related to both the glass transition temperature and the Kauzmann catastrophe temperature. At $T < T_K$, the entropy of supercooled liquid computed by extrapolation of high-temperature data is *less than* that of its corresponding crystal (the Kauzmann Paradox). The computed TVF viscosity (Eqn (5.5)) explodes toward an infinite singularity as $T \to T_K$. The relationship between the TVF and the Arrhenian model is found by examining the temperature derivative of the viscosity. In the Arrhenian model, $\partial \ln \eta_{Arr}/\partial(1/T) = E_A/R$ whereas for a TVF fluid $\partial \ln \eta_{TVF}/\partial(1/T) = BT^2/(T - T_K)^2$. Thus, in the limit $T_K \to 0$, the TVF and the Arrhenian models are identical with $B = E_A/R$. In general, T_K is close to but usually somewhat less than T_g, the glass transition temperature. Typically, T_g for geosilicate compositions is ~1000 K. T_g for pure silica is somewhat higher (1500 K).

The TVF model therefore shows that the variation in melt viscosity with reciprocal temperature decreases as temperature increases and is not a constant (E_A) as in the Arrhenian model. The TVF empirical model draws some theoretical foundation from the Adams–Gibbs–DiMarzio (AGD) configurational entropy model. In AGD, viscosity depends on temperature according to

$$\eta = \eta_o \exp\left(D/TS_{conf}(T)\right) \tag{5.6a}$$

where S_{conf} is the configurational entropy of the melt. S_{conf} includes a contribution computed from liquid and glass isobaric heat capacity data, as well as the residual entropy of glass (frozen liquid) at the glass transition temperature, T_g. The value of $S_{conf}(T)$ is computed from

$$S_{conf}(T) = \int_{T_K}^{T} \frac{\Delta C_p(T)}{T'} dT' \tag{5.6b}$$

where the heat capacity term in Eqn (5.6b) is the experimentally observed difference in liquid and solid heat capacities. The parameter D is temperature independent but varies with composition. An important aspect of the AGD theory is that it connects thermodynamic and transport properties. It is based on a theory of cooperative behavior during dynamic rearrangement of atomic configurations in the liquid state. The AGD theory collapses to the empirical TVF expression provided the heat capacity difference is given by the hyperbolic expression $\Delta C_P(T) = \frac{CT_K}{T}$ in Eqn (5.6b). Although this identification is one of several possibilities, the collapse of the AGD expression to the TVF provides some theoretical support for the validity of the otherwise empirical TVF formulation.

An empirical model that gives melt viscosity as a function of composition and temperature based on the TVF formulation has been calibrated and in wide use (Giordano et al., 2008). This empirical model gives the added benefit of providing estimates of the glass transition temperature and melt fragility as a function of melt composition at low pressure. Pressure effects are not considered in the present form of this model, however. The Arrhenian pressure correction can be used to roughly account for pressure by simple extension of the TVF. For less precise work, the Arrhenian model still finds application because it is so simple to implement, although extrapolating beyond the bounds of the experimental measurements is risky at best. The viscosity of naturally occurring silicate melts can span over 10 orders of magnitude due to variations in composition and temperature (Table 5.1 and Figure 5.4). Dissolved water is especially effective in lowering the viscosity of polymerized melts (e.g., three orders of magnitude with addition of 3 wt H_2O for rhyolite melt), while it has comparative small effects on the viscosity of depolymerized (mafic and ultramafic) liquids (see Figure 5.5).

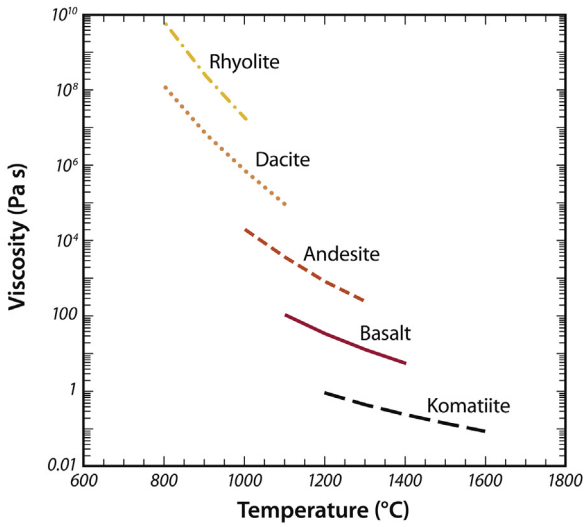

FIGURE 5.4 Viscosity as a function of temperature at 1 bar (10^{-4} GPa) for natural melts spanning the compositional range rhyolite to komatiite. All compositions are volatile-free. The temperature range is illustrative of typical eruption temperatures for each composition.

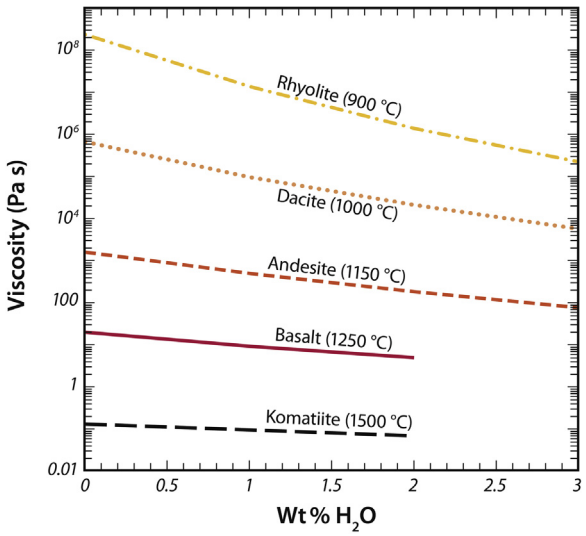

FIGURE 5.5 Melt viscosity as a function of dissolved water content for natural melts spanning the range rhyolite to komatiite. Temperatures for each composition are characteristic eruption temperatures. Viscosities are calculated for pressure equal to 1 bar (10^{-4} GPa). For the rhyolite composition, two different models are shown. Note the very dramatic effect of dissolved water on the viscosity of natural melts. Viscosity models are from Shaw (1972) and Giordano et al. (2008).

4.2. Magma Viscosity

Far fewer data exist on the rheological properties of magmatic suspensions compared to silicate melts. Magma, a mixture of suspended crystals and vapor bubbles in a melt matrix, may be expected to exhibit complex rheological behavior when significant amounts of suspended crystals and bubbles ("particles") are present. Silicate foams,

defined as concentrated emulsions with porosity greater than about 60 volume percent ($\phi > 0.6$) are found in small quantities at virtually all volcanic centers because magma typically contains volatiles (0.1–10 wt%) and the common volatiles (H_2O and CO_2) are practically insoluble in melts at low pressure. Magma decompression during magma ascent commonly leads to volatile saturation. The important variables governing the viscosity of multiphase mixtures include the shear rate, the volume fraction of solid and bubbles, the size and shape distributions of these "particles" (solids and bubbles), temperature, pressure, and melt viscosity. There are no experiments exploring the rheological properties that account for these variables collectively and comprehensively although some effects, such as the effects of variable solid loading fractions, have been explored. A complication is that in natural systems the flow itself influences the distribution of particles via mechanical (sorting) and thermal effects. For example, viscous forces acting on particles can cause their movement relative to melt and each other, e.g., flow differentiation. A heterogeneous distribution of particles can evolve from an initially homogeneous distribution under the influence of particle-melt viscous drag and pressure forces. Similarly, thermal gradients can effect the local concentration of phenocrysts thereby modifying velocity gradients. The rheology of multiphase fluids is complex and currently the subject of intensive study. Fortunately, there has been some progress on two-phase mixtures (both crystal-melt suspensions and melt-vapor emulsions) applicable to magmatic systems. These studies enable one to approximate the viscosity of magmatic suspensions when suspensions are composed of monosized "particles" in the creeping flow regime at very low rates of shear. These models are valid from the dilute limit to the random packing volume fraction limit of $\phi \approx 0.64$.

To first order, the effect of increasing the volume fraction of crystals, ϕ, in a melt is to increase the relative viscosity, η_r, according to

$$\eta_r = \eta_{mix}/\eta_{melt} = (1 - \phi/\phi_o)^{-5/2} \qquad (5.7)$$

where η_{mix} is the viscosity of the crystal–liquid suspension or mixture, η_{melt} is the viscosity of aphyric melt, and ϕ_o is the maximum packing fraction of the solid. Equation (5.7) shows that the loading level of crystals is limited by ϕ_o, the geometric limit for contact of solids in the most efficient packing arrangement. For rhombohedral packing of spherical particles, $\phi_o = 0.74$ whereas for simple cubic packing and body-centered cubic packing $\phi_o = 0.52$ and 0.60, respectively. In practice, random packing of spheres generally gives ϕ_o in the range 0.60–0.65. Equation (5.7) shows that the volume fraction and the maximum packing fraction ϕ_o of solids are the two important parameters governing the viscous response of magma. Polydispersity, the presence of a nonunimodal distribution of particles, tends to reduce the viscosity of a magma at a fixed ϕ because smaller particles can fit in between the larger ones. The viscosity of a unimodal crystal-bearing magma with $\phi = 0.3$ is about 10 times higher than its value for the melt phase alone based on Eqn (5.7). In more detail, it is both the size and shape variation of individual crystals, as well as the overall structure of the mixture, that strongly controls rheological properties. An alternative model that purportedly accounts for the presence of melt entrapped between particles gives smaller relative viscosities compared to Eqn (5.7). The expression is

$$\eta_r = \frac{\eta_{mix}}{\eta_{melt}} = \left(1 - \frac{\phi}{\phi_o}\right)^{-C_1\phi_o} \qquad (5.8)$$

where the C_1 equals 2.5 and ϕ_o represents the random close packing limit. The parameters C_1 and ϕ_o vary depending on the particle size and shape distributions. For nonspherical particles, C_1 is larger than the Einstein value of 5/2, used in Eqn (5.7). For high shear rates, some particle arrangements can form where spherical particles tend to form clusters and the mixture is capable of flow at volume fraction that exceeds the zero shear rate limit $\phi_o \approx 0.64$. Presently, the most accurate model for a unimodal, solid + melt suspension at zero shear rate is

$$\eta_r = \frac{\eta_{mix}}{\eta_{melt}} = \left(\frac{1 - \phi}{1 - \frac{\phi}{\phi_o}}\right)^{\frac{C_1\phi_o}{1-\phi_o}} \qquad (5.9)$$

Values for C_1 and ϕ_o suitable for **magma rheology** calculations accounting for nonspherical crystals and the close pack limit are 3 and 0.64, respectively. Some typical relative suspension viscosities as a function of solid volume fraction are shown in Figure 5.6 based on Eqns (5.7)–(5.9) for creeping flow (low shear rate) of a suspension of rigid spherical monodisperse particles with the packing limit $\phi_o = 0.64$. Also shown is an approximation to the more realistic case of inequant particles based on Eqn (5.9) with $C_1 = 3$. At high-volume fraction solids, these various models exhibit order of magnitude differences in the relative viscosity—small variations in C_1 and ϕ_o amplify these differences.

In noncreeping flows, a nonlinear relation exists between the shear stress sustained by the mixture and the shear rate. Such suspensions exhibit power-law behavior. On a plot of shear stress versus shear rate, the tangent at a given shear rate is the effective viscosity of the suspension at that shear rate. Because the effective viscosity is a monotonically decreasing function of shear rate at fixed temperature and solid fraction, a value for the yield stress can sometimes be approximated by extrapolation of the tangent to the locus of points in the shear stress–shear rate plane to the stress axis at zero shear rate. More experimental work is required to

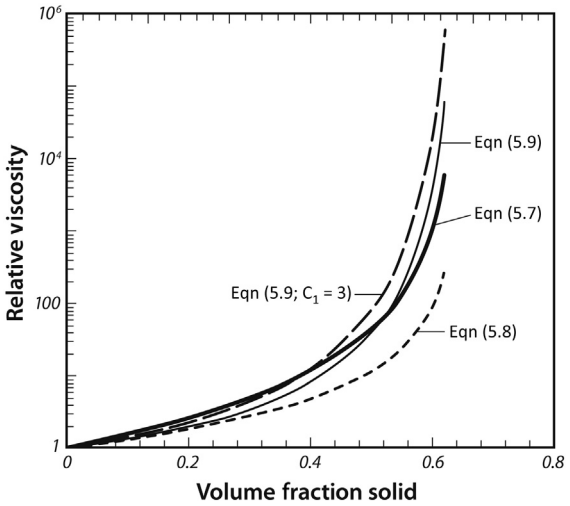

FIGURE 5.6 Relative viscosity of magmatic suspensions containing solids as a function of volume fraction of solids. The models refer to Eqns (5.7)–(5.9). Note the congruity of models for low crystal loading volume fraction and the divergence as the close packing limit of ~0.64 is approached. Relative viscosity models from Brouwers (2010). The coefficient $C_1 = 3$ allows for particle nonsphericity, approximately based on Eqn (5.9).

develop quantitative expressions that relate volume fraction solid to the apparent yield stress. In the meantime, Eqn (5.9) may be used as an approximation keeping in mind its inherent limitation to low shear rate flows.

In bubble-melt mixtures, λ viscosity can be either an increasing or decreasing function of the volume fraction of the low-viscosity phase (ϕ) depending on the rate at which the mixture is sheared. At low rates of shear ($\dot{\gamma}$), bubbles act as nondeformable inclusions and η_r increases with increasing ϕ similar to when solids (e.g., crystals) are added to melt. In distinction, at high shear rate, low-viscosity bubbles readily deform and the mixture viscosity decreases with increasing bubble fraction. A dimensionless parameter termed the capillary number (Ca) is useful in determining the appropriate rheodynamic regime. The capillary number is defined $Ca = \frac{\eta\dot{\gamma}r_b}{\sigma}$ where η, $\dot{\gamma}$, r_b, and σ represent the melt viscosity, shear rate, bubble radius, and melt-vapor interfacial tension, respectively. The capillary number can be thought of as the ratio of viscous tractions acting on the boundaries of a bubble that distort it from a spherical shape relative to interfacial surface forces that tends to preserve its spherical shape. Small values of Ca correspond to conditions where surface tension dominates and bubbles retain their spherical shapes. This is favored in finely dispersed (small bubble size), low-viscosity emulsions subjected to low rates of deformation. One expects a relative viscosity relation of the form $\eta_r = f(\phi,Ca)$ such that for small capillary number (roughly $Ca < 1$), η_r is an increasing function of ϕ. In contrast, for regimes with $Ca > 1$, the relative viscosity decreases with increasing bubble content. Natural systems span the range from $Ca < 1$ to $Ca \gg 1$ so it is important to consider the dynamic regime when considering the effect of bubbles on the viscosity of magma. Relative viscosity can drop by a factor of 10 as the bubble content increases from 0 to ~50 volume percent in the high Ca regime.

Self-organization of dispersed particles (solids or bubbles) to form structured mixtures can give rise to large spontaneous changes in viscosity during flow. The formation of structure has been observed in laboratory models and probably quite relevant during flow of crystal slurries or vesiculated magma in chambers and conduits. Further experimental, analytical, and numerical work is needed to quantify the rheology of magmatic crystal-melt-vapor suspensions.

4.3. Thermal Conductivity

Transport of magmatic heat occurs by several mechanisms including convection (heat transported by bulk flow), phonon conduction (heat transported by atomic vibration), and radiation (an electromagnetic phenomenon involving photon transfer). Radiation travels through a vacuum at the speed of light; most gases are transparent to radiation. Radiative transport of heat may be important in transition metal poor melts due to their relative transparency. Since most gases are transparent, radiative heat transfer may also be important across bubbles in magmatic emulsions and foams. In contrast, radiative heat transport can generally be ignored in mafic melts containing significant amounts of transition metals (e.g., Fe, Ti, Ni) because such melts are relatively opaque to thermal radiation, i.e., the mean free photon path is relatively short—on the order of millimeters. The photon (radiative) conductivity (k_R) can be approximated in this case as

$$k_{rad} = \frac{16}{3}\sigma n^2 T^3 \Lambda \qquad (5.10)$$

where σ is the Stefan–Boltzmann constant (5.67×10^{-8} J/m^2 K^4 s), n is the index of refraction, and Λ is the mean free path for photons. The thermal transfer by photons depends on Λ as well as the emissivities of the surfaces across which heat is being transferred. When $\Lambda \sim 0$ (as in an opaque melt) or when one is concerned with transport of heat across distances much larger than Λ, radiative transfer is negligible. It is only when Λ is relatively large, as in transparent high-silica melts or in transparent vapor-melt emulsions that photon conduction may become appreciable. Because geometric factors are often relevant, the importance of radiative heat transfer in geological processes (as opposed to laboratory small-scale experiments) should be carefully considered.

The phonon thermal conductivity (k) provides a quantitative measure of the importance of phonon heat

conduction in solids and melts. The thermal diffusivity (κ) defined $\kappa = k/\rho C_p$ is the relevant parameter in transient heat conduction problems. The thermal diffusivity involves a combination of thermodynamic properties and the phonon thermal conductivity. Quantized thermal waves called phonons carry heat in silicate crystals, glasses, and melts. Thermal resistivity (W), which is inversely proportional to thermal conductivity (i.e., $k \propto W^{-1}$), arises due to both phonon–phonon interaction and structural disorder. Because disorder is an outstanding characteristic of the glassy and molten state, one may expect the mean free path for the dominant thermal phonons to approximately equal the scale of structural disorder, roughly 0.3–0.6 nm in a typical silicate glass or melt. The thermal conductivity of a solid or melt may be estimated according to the relation

$$k = \frac{1}{3}\rho C_V c \Lambda \tag{5.11}$$

where Λ is the phonon mean free path length, c is the sonic velocity (several kilometers per second), ρ is the melt density and C_V is the isochoric specific heat capacity. Because the structure of a melt or glass is sensitive to pressure, one might anticipate the mean free phonon length and hence k (other factors constant) to increase with pressure. In general, for a silicate liquid k decreases as temperature increases but increases as pressure increases, consistent with expectations (see Table 5.2).

Because radiative transfer tends to dominate at high temperatures, it can be difficult to cleanly separate the effects of phonon conduction from radiative transfer in laboratory experiments. There are surprisingly few reliable measurements of the thermal conductivity of liquid silicates, fewer for geochemically important compositions, and virtually no laboratory data regarding the effects of pressure on phonon conduction. Fortunately, within the past few years, there have been some important advances. Values for the phonon thermal conductivity of some geosilicate liquids, glasses, and crystals for a range of temperatures and pressures are given in Table 5.2 (Tables S5.8 and S5.9 provide more exhaustive compilations). These data show that as temperature increases, the thermal conductivity typically decreases for both solids and liquids. Values if k for silicate liquids lie in the range 0.8–1.6 W/m K with k generally higher from more polymerized liquids. Finally, very recently, phonon conductivities for molten $NaAlSi_3O_8$, $CaMgSi_2O_6$, and Mg_2SiO_4 have been determined from MD simulations in the range 2000–5000 K and 0–30 GPa (Tables 5.2 and S5.9). Values for molten albite and diopside at 0 GPa agree well with laboratory measurements at 1 bar, and confirm a weak negative temperature dependence of k at constant pressure. They further show that at constant temperature, k increases rather significantly as pressure increases. These relationships have important implications for the efficiency of heat transfer associated with molten regions of the mantle.

4.4. Diffusion

Mass is transported in magmatic systems by bulk flow (advection) and by diffusion. Their operation separately and collectively is responsible for convection in magma bodies. There is an extensive body of information pertaining to diffusion in silicate melts and glasses as a function of temperature, composition, and, to a lesser extent, pressure. This is due in large measure to myriad industrial and materials processing applications of diffusion as well as the importance of diffusion in petrologic processes such as crystal nucleation and growth, the growth of vapor bubbles, the homogenization of melt inclusions, the resetting of geochronological clocks, and the mixing of magmas. There is a deep connection between the atomic structure of a melt or glass and the mobility of its constituents. Hence study of the systematics of diffusion bridges the gap between the microscopic and macroscopic realms relevant to magma transport phenomena. Several excellent reviews of diffusion for both industrial and geological materials are available and listed in Further Reading. In this section, the types of diffusion important for magmatic systems are reviewed and typical values are given to indicate the main trends and orders of magnitude. We review theory and highlight applications of these data. Since we are mainly concerned with magmatic systems discussion is limited to properties for the liquid state, i.e., temperatures above the glass transition ($\eta < 10^{12}$ Pa s).

Diffusion involves the motion of different constituents at the molecular or atomic scale leading to local (inter) mixing or net transport of mass. From an atomistic standpoint, diffusion is the consequence of the random walk of particles, often thermally activated, that depends on temperature, the size and charge density of the diffusing species, and the viscosity of the surrounding medium. Motion by random walk determines the intrinsic mobility of the diffusing species and is described by the self-diffusion coefficient (D*). The pathways for random walk (self-diffusion) cannot be measured directly in the laboratory; however, approximate values can be obtained by tracking the rate of transfer of readily identifiable components that are either chemically indistinguishable, i.e., different isotopes of a given element, or elements that are in such dilute concentration that their presence has no resolvable effect on the concentration of other components. The term intradiffusion is used to describe the bidirectional exchange of isotopes of major, minor, or trace elements in an otherwise homogeneous system, while the term tracer diffusion is reserved for cases where a trace element (or one of its isotopes) diffuses solely down its own concentration

gradient. Both are commonly assumed to be equal measures of self-diffusion provided (1) a constant activity coefficient—which in the case of trace diffusion means the tracer obeys Henry's law (the concentration limits for Henrian behavior must be determined empirically, but is commonly <1000 part per million), (2) pathways for diffusion are the same as for random walk, and (3) there are no significant mass-dependent (isotope) effects. There are instances where these essential requirements are not met and here diffusion coefficients provide at best semi-quantitative constraints on intrinsic mobility in natural systems only in so far as they mimic laboratory conditions.

More commonly in natural systems diffusion arises from and occurs in the presence of chemical (potential) gradients due to non-Henrian behavior of the tracer or concentration gradients of other components at some location and time. This is referred to as chemical diffusion and is distinguished by simultaneous fluxes of components. From a phenomenological perspective, the chemical flux of a given component can be described by Fick's first law relating the net flux of that component to a negative gradient in its chemical potential or activity. Where chemical diffusion involves just two components of a multicomponent system a simple binary solution to Fick's law is sufficient; however, if there are net displacements of more than two components a full description of chemical diffusion requires a $(n-1)$ by $(n-1)$ diffusion matrix with elements D_{ij}. That is, for an n-component system, the flux of the ith component depends on the chemical potential gradient of any independent set of $n-1$ components and not simply the ith component. Because the chemical diffusion rate of the ith component depends on $n-1$ chemical potential gradients whereas isotopic equilibration of the ith component depends on the self-diffusivity of that species, decoupling between elemental and isotopic concentrations is possible. Furthermore, due to nonideality and/or diffusive coupling effects, even for ideal solutions, chemical diffusion can involve a net flux of elements up, rather than down, their concentration gradients. This is referred to as uphill diffusion and is well documented in experiments. In nature, enrichment in K_2O along the granite/gabbro interface and biotite-rich rinds often surrounding mafic enclaves in granitic or granodioritic magma has been attributed to uphill diffusion.

In recent years, there have been a number of experimental studies of chemical diffusion involving three and four component systems (e.g., $CaO-MgO-Al_2O_3-SiO_2$) that have succeeded in constraining the full diffusion coefficient matrix. These studies have shown that the on-diagonal D_{ii} correspond closely to self-diffusivities, while the off-diagonal terms are typically smaller, although not always the case, and commonly negative, which can lead to uphill diffusion. Given the challenges constraining the diffusion coefficient matrix for even up to four components it is not likely that this approach will have much practical utility for modeling natural magmatic systems $(n \gg 4)$ anytime soon.

An alternative and much simplified approach is to treat chemical diffusion in magmas as an effective binary process. This is possible when chiefly the component of interest varies in concentration relative to all other components in the system. In the limit of Henry's law this is tracer diffusion. However, once the concentration exceeds the Henrian limit, the flux is no longer controlled solely by the magnitude of the concentration gradient, but in how the activity of the species changes along that gradient—this is the domain for chemical diffusion. The effective binary diffusion approach has also been used to quantify interdiffusion between vastly different magmas (such as basalt and rhyolite) where often the diffusion of SiO_2 (Si and O being the slowest diffusing elements) is considered relative to all the other components or where all the network formers (Si, Al, Fe^{+3}, etc.) are lumped together as one component and all the network modifiers (Fe^{+2}, Mg, Ca, Na, and K in excess of that needed to charge balance tetrahedral Al, Fe^{+3}, etc.) are combined as the other. While again the diffusivities determined by this approach are only applicable to natural systems in so far as the laboratory conditions simulate nature, effective binary diffusivities especially for SiO_2 or network formers do place limits on the length and timescales for chemical homogenization during magma commingling. This enables us to evaluate how species with high intrinsic mobility are locally redistributed by chemical diffusion within the more sustained major element gradient due to sluggish diffusion of network-forming cations and oxygen (Figure 5.7). Consider the diffusive length during the 10^5 year solidification time of a 10^3 km^3 gabbroic pluton (characteristic length ~ 10 km). For O and Si, diffusion can effect changes in concentration over ~ 3 m, while in the case of Li and H_2O having diffusivities two to three orders of magnitude larger diffusive exchange can occur over ~ 60 m. Possible ramifications for isotopic composition of fast and slow diffusion species such as Sr and Nd, respectively, are illustrated in Figure 5.8.

Nearly 65 years ago L.S. Darken proposed that the chemical diffusivity D_i^c can be expressed as

$$D_i^c = kTM_i\left[1 + \frac{d \ln \gamma_i}{d \ln x_i}\right] \tag{5.12}$$

where k is the Boltzmann constant, T is temperature, γ_i and x_i are the activity coefficient and mole fraction of species i, respectively, and M_i is the intrinsic mobility (velocity of species i per unit force). Equation (5.12) provides an explicit expression relating the chemical diffusivity to both species i intrinsic mobility (random walk velocity) and its activity gradient causing a directional flux. Consider first the case of uniform composition. Since there is no chemical

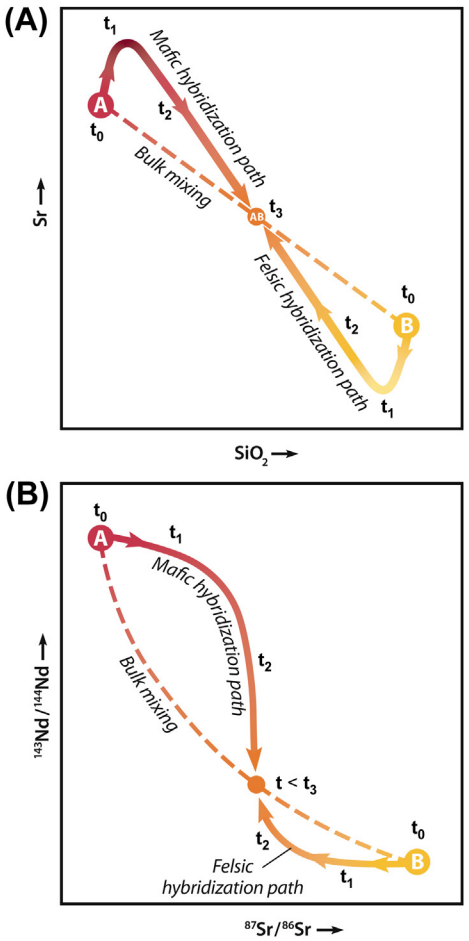

FIGURE 5.7 Schematic diagram showing progressive hybridization of mafic (A, red) and felsic (B, yellow) magmas when mixing is limited by a large viscosity contrast and diffusion. (A) Solid curves with arrows show the paths for the mafic magma (upper trajectories) and complementary felsic magma (lower trajectories) as a function of time leading eventually to bulk homogenization in time t_3. These trends deviate markedly from those predicted for simple binary mixing shown by the dashed curves. Uphill diffusion of Sr is depicted when the gradient in activity is opposite to the gradient in concentration, negative Darken diffusivity (see text). In (B) the covariation of $^{87}Sr/^{86}Sr$ and $^{143}Nd/^{144}Nd$ ratios reflects the fact that the intrinsic mobility of Sr is greater than of Nd (see Tables S5.10 and S5.11). Isotopic equilibrium is practically achieved in time t, which may be less than that required for the system to achieve complete chemical homogenization (t_3). *Modified after Figure 2 in Lesher, C.E., 1990. Decoupling of chemical and isotopic exchange during magma mixing. Nature 344, 235–237 with permission Nature Publishing Group.*

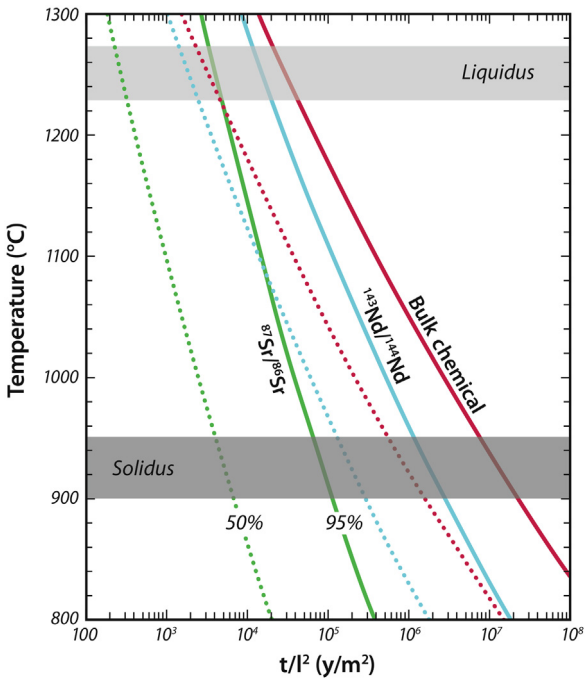

FIGURE 5.8 Effects of temperature, time, and diffusion length scale for Sr and Nd isotopic homogenization and bulk chemical homogenization of basalt with entrained blobs of rhyolite. Diffusive impedance is the time (t) in years over the length scale of the compositional heterogeneity (l) in meters squared, t/l^2, is the diffusive impedance. Contours for 50 and 95% of the way to complete homogenization of isotopic composition and bulk chemical composition are represented by the dotted and solid curves, respectively. Approximate liquidus and solidus temperatures indicated by stippled horizontal bars delimiting the temperature interval where hybridization of basalt is likely to occur. *Modified after Figure 12 in Lesher, C.E., 1994. Kinetics of Sr and Nd exchange in silicate liquids – theory, experiments, and applications to uphill diffusion, isotopic equilibration, and irreversible mixing of magmas. Journal of Geophysical Research 99, 9585–9604 with permission from John Wiley & Sons Publications.*

flux, $\frac{d \ln \gamma_i}{d \ln x_i} = 0$ and $D_i^c = kTM_i$. This is tantamount to our definition of self-diffusivity, D^*, so that

$$D_i^c = D_i^* \left[1 + \frac{d \ln \gamma_i}{d \ln x_i}\right] \tag{5.13}$$

Now consider species i present in dilute concentration and obeying Henry's law, i.e., $\gamma_i =$ constant. In this case, while $d\ln x_i$ is nonzero, $d\ln\gamma_i$ will be zero and thus $\frac{d \ln \gamma_i}{d \ln x_i} = 0$.

Herein lies the common assumption that tracer diffusion and self-diffusion are equivalent measures of intrinsic mobility—but again only in the limit of Henry's law.

The equivalency of the self-diffusion and intradiffusion as might be derived from an isotope diffusion couple experiment is not so straightforward, since isotopes of the same element have mass differences and thus their self-diffusivities may differ. Drawing again on Darken's work, the diffusivity for exchange of two isotopes of the same element (isotope 1 with mass m_1 and isotope 2 with mass m_2) in an otherwise homogeneous solution depends on their relative concentrations and self-diffusivities

$$\overline{D} = x_1 D_2^* + x_2 D_1^* \tag{5.14a}$$

where

$$D_1^* = D_2^* \left(\frac{m_2}{m_1}\right)^{\beta} \tag{5.14b}$$

β is typically 0.5 for gases but markedly smaller for condensed phases. In the case of silicate melts, ^{6}Li has been shown to diffusive ~12% faster than ^{7}Li giving $\beta = 0.2$, while the differences in diffusivities of isotopes of Fe, Mg, and Ca are well below 2%, constraining $\beta < 0.06$ for these elements. β for Si is expected to be markedly smaller ($\leq$0.025) meaning that differences in self-diffusivities for Si isotopes are likely far too smaller to be resolved by current mass spectrometry methods. Furthermore, from Eqn (5.14b) it can be appreciated that as $\frac{m_2}{m_1} \rightarrow 1, D_1^* \rightarrow D_2^*$ so that for most petrologic applications involving traditional radiogenic systems (Sr, Nd, Hf, and Pb) the differences in isotope self-diffusivities will be so small that diffusive fractionation effects will be negligible. On the other hand, this also means that, in practice, the self-diffusivity can be determined directly by measuring the flux of one isotope relative to others of that element in an otherwise homogeneous medium—in other words, from an intradiffusion couple experiment.

Returning to Eqn (5.13), in most situations encountered in magmatic systems the ratio $\frac{d \ln \gamma_i}{d \ln x_i}$ will have a value other than zero, while its magnitude is expected to vary in space and time. Thus, the Darken diffusivity has the peculiarly feature of being either positive, negative, or zero depending on whether the activity of species *i* increases, decreases, or is constant with concentration, respectively. While the former case is usually encountered and certainly prevails in the absence of gradients in other components, the latter situations arise due to strong nonideality accompanying gradients in other components, particularly silica content. The occurrence of uphill diffusion in this context can then be appreciated as a direct consequence of a negative Darken diffusivity for that element, while for rapidly diffusing species concentration differences can be established essentially under quasi-equilibrium conditions where the activity gradient tends to zero. These concentration differences can persist as long as there remain differences in, for example, silica content. The main point regarding magma mixing is that ultimately mass transfer depends on chemical diffusion operating at the molecular scale. The process is generally not explicable by linear mixing, and due to differences in self-diffusivities and the complexities of the activity–composition relations significant decoupling among chemical components and isotopic systems is possible (Figures 5.7 and 5.8). Armed with this appreciation can help in deciphering the often complex compositional relationship among hybrid rocks formed by magma mingling.

A great deal is known about the effects of temperature and composition on self/tracer and effective binary chemical diffusivities at atmospheric pressure, while our understanding of the effects pressure is meager. Following from Eqn (5.4), the Arrhenius relation can also describe the dependence of diffusivity on pressure and temperature

$$D = D_0 \exp[-(E_a + PV_a)/RT] \qquad (5.15)$$

where D_0 is constant for a fixed composition, and E_a and V_a represent the activation energy and activation volume for diffusive transport, respectively. Equations (5.15) is a useful starting point for any analysis of the temperature and pressure dependence of diffusivities; however, certainly in the case of silicate melts the assumption of constant E_a and V_a may only be valid for restricted temperature and pressure intervals—for many of the same reasons that Eqn (5.4) fails for fragile liquids. However, for diffusion the preexponential term (D_0) depends strongly on melt composition and the size and charge of the species. As such, Eqn (5.15) often does not provide sensible results if the diffusivities being considered are chemical diffusivities that depend on the details of the compositional gradients used to determine D_{ij}. It is best to limit consideration to experimental measurements that serve as good proxies for self-diffusivities, i.e., tracer and intradiffusivities (see Tables S5.10 and S5.11). E_a is found to be of order 300–400 kJ/mol for network-forming atoms like Si and Al and in the range 250–180 kJ/mol for transition metals and the alkaline earth metals. Alkali metals have activation energies in the range 120–220 kJ/mol.

Less is known about V_a for silicate melts. V_a is typically positive for network modifiers such as Ca and Mg (+2 to +12 cm^3/mol) and can be positive or negative for network-forming cations (Si) and oxygen, depending on composition and pressure. Positive V_a is consistent with more conventional free-volume models of ionic diffusion, while to explain negative V_a one often appeals to cooperative modes of diffusion. For basalt to rhyolite compositions at low to moderate pressures, V_a for Si and O range from −2 to −15 cm^3/mol with more negative values associated with more silicic (polymerized) melts. Both experiments and MD simulations show that V_a for Si and O can change from negative to positive at high pressure. The maximum in the diffusivity has been attributed to progressive stabilization of high coordinated network species with pressure, but there is also mounting evidence that the anomalous pressure dependence of network formers up to 5–6 GPa is intimately connected to the compressible nature of polymerized silicate melts over this pressure range. In contrast, V_a for Si and O is positive even at low pressure in depolymerized nature liquids such as diopsidic melt suggesting that given their more compact structure diffusion is restricted by available free-volume and more readily accomplished by motion of individual ions rather than through cooperative motion. Granted, these expectations are based on limited data for

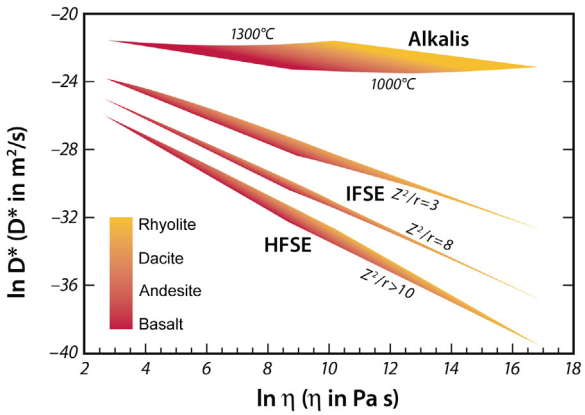

FIGURE 5.9 Tracer diffusivities for the alkalis, intermediate field strength elements (IFSE bounded by $Z^2/r = 3$ and 8) and high field strength elements (HFSE; $Z^2/r > 10$) from 1300 °C (upper bound) to 1000 °C (lower bound) and spanning composition of basalt (red, left hand bound) to rhyolite (yellow, right hand bound) computed from equations presented by Mungall (2002). Diffusivities are plotted against log viscosity from Giordano et al. (2008).

high-pressure conditions and further laboratory measurements and first-principle calculations are sorely needed to reliably constraint processes involving diffusion in the deep interior of our own and other planetary bodies. Studies of diffusion in conjugation with viscous flow are also critical for understanding the connections between these transport processes on a fundamental physical/structural level.

Roughly, E_a and V_a for oxygen self-diffusion in a melt are equivalent to E_A and V_A for viscous flow because viscous flow in a silicate melt is ultimately related to the mobility of oxygen, the predominant constituent. This expectation derives from the classic expressions proposed by Einstein, Glasstone, Eyring, among others, that assume $D \propto \eta^{-1}$. This simple proportionality has been very useful in understanding relative magnitudes of self-diffusivities and their dependence on magma composition (Figure 5.9). As a rule, oxygen together with Si and other high field strength cations tend to have the smallest self-diffusivities for a given temperature and melt composition, while diffusivities for the transition, alkaline earth, and alkali metals are uniformly larger. In general, network-modifying ions of high charge and large size have smaller self-diffusivities than small ions of low charge, other factors remaining the same. For example, in a basaltic melt at 1300 °C, oxygen and the network cations Si and Al have $D^* \sim 3 \times 10^{-12}$ m^2/s. This compares with rare earth and transition metals (e.g., Fe, Ti), and alkaline earths (e.g., Mg, Ca, Sr, Ba) for which $D^* \sim 1 \times 10^{-11}$ m^2/s and $\sim 2 \times 10^{-11}$ m^2/s, respectively. A typical ranking for basaltic melts is $D^{Ba} \geq D^{Sr} > D^{Ca} > D^{Mg} > D^{Fe} > D^{REE} > D^{Ti}$. The alkalis are significantly more mobile with $D^* \sim 3 \times 10^{-10}$ m^2/s and exhibit a strong dependence on ionic radius with $D^{Li} \geq D^{Na} > D^{K} > D^{Rb} > D^{Cs}$. The diffusivity of the carbonate group (CO_3) is $\sim 1.2 \times 10^{-10}$ m^2/s whereas for H_2O, $D = \sim 1 \times 10^{-9}$ m^2/s, and depends on the concentration of dissolved water. At fixed temperature, D*'s for oxygen and most high field strength cations, including Si, are larger in basalt melt compared to rhyolite, by a factor of 5–500; but interestingly the alkalis shown little to no dependence on magma composition. These relationships are illustrated in Figure 5.9 using an empirical model based on the assumption that $D \propto \eta^{-1}$ and fit to experimental data for self-diffusion and independent constraints on viscosity. While such empirical models do have limitations, notably missing is a comprehensive picture of the effects of volatile species (H_2O, CO_2, etc.) and pressure, they do permit order of magnitude estimates of self-diffusivities for ions of different size and charge over a broad range of natural magma compositions and temperature. This information is essential for modeling the dynamics and timescales of magmatic processes fundamentally controlled by diffusion at the molecular to atomic length scales.

5. CONCLUSIONS

The important thermodynamic and transport properties of magma have been reviewed in this chapter. The complete description of multicomponent and multiphase magma at temperatures from 800 to 5000 K and pressures from 10^{-4} GPa (surface) to 135 GPa (base of mantle) is an ambitious program that will take many years to accomplish. Although an enormous task, there are reasons to be optimistic. Within the last quarter century, knowledge of the thermodynamic properties of high-temperature crystalline, molten, and glassy silicates including melts of natural composition has grown dramatically. Although still far from complete, thermodynamic properties for many crystalline phases relevant to magmatic systems are known at the high temperature and pressure conditions extending at least to the base of the lithosphere and within the asthenosphere where primary liquids are formed beneath spreading ridges, within upwelling mantle plumes and at subduction zones. An approximate model for the Gibbs free energy of natural silicate liquids has also been developed in the past 15 years and is undergoing continuous revision and expansion. These advances have improved efforts to describe and predict equilibrium phase relations involved in the melting and solidification of magma. Similarly, studies of the temperature, pressure, and composition dependence of melt viscosity, the rheology of magmatic (solid–melt–vapor) mixtures, chemical, tracer, and self-diffusion and thermal conductivity have been made for a variety of natural and synthetic melts and glasses. Correlations have been developed for some properties valid in specific regions of temperature–pressure–composition space that enable one to obtain order of

magnitude or better estimates of many critical properties. These have been greatly aided by significant advances in experimental techniques, especially for high pressures and utilizing a variety of radiation sources and spectroscopic tools, and analytical methods that are probing at ever smaller length scales with hitherto unfathomable precision and accuracy. Development of models based on condensed matter physics has come to supersede earlier purely empirical models and provide for rational interpolations and a basis for careful extrapolation. In the computational realm, MD simulations are increasingly being applied to investigate the structure and properties of molten silicates at very high temperatures and pressures. This method, which involves use of a potential energy expression describing the electrostatic interactions between the various atoms in a fluid or melt, enables one to compute thermodynamic, spectroscopic, and transport properties under a variety of conditions. Although properties so computed are estimates, they do provide a means for understanding, at the atomic level, the effect of temperature, pressure, and composition on physical properties and for identifying critical laboratory experiments that should be performed.

Study of the properties of molten, glassy, and high-temperature crystalline silicates and oxides of geological relevance is a burgeoning field for last research. The rate of acquisition of new information is accelerating as new techniques are applied to old problems. There are hundreds of volcanic eruptions each year and many of these present dangers involving the loss of life and property. The first step in taming magma is to understand its nature from a fundamental and broad perspective. At the same time a deeper understanding of the evolution of planet Earth and, by analogy, other terrestrial planets both within our solar system and beyond depends on knowledge regarding the physical properties of magma.

SUPPLEMENTARY MATERIAL FOR THERMODYNAMIC AND TRANSPORT PROPERTIES OF SILICATE MELTS AND MAGMA

TABLE S5.1 Partial Molar Volumes, Thermal Expansions and Compressibilities of Oxide Components. Note That $(\partial V_i/\partial P)_T \equiv -\beta_T V_i$, Where β_T Is the Isothermal Partial Molar Compressibility of the ith Component and $(\partial V_i/\partial T)_p \equiv \alpha_P V_i$, Where α_P Is the Isobaric Expansivity.

$$V_{liq}(T,P,X) = \Sigma X_i \left[V_{i,1673K} + (\partial V_i/\partial T)_p (T-1673) + (\partial V_i/\partial P)_T P\right]$$

	$V_{i,1673K}$ (10^{-6} m^3/mol)	$(\partial V_i/\partial T)_P$ (10^{-9} m^3/mol·K)	$(\partial V_i/\partial P)_T$ (10^{-6} m^3/mol·GPa)
SiO_2	26.86 ± 0.03	0.0	−1.89 ± 0.02
TiO_2	23.16 ± 0.26	7.24 ± 0.46	−2.31 ± 0.06
Al_2O_3	37.42 ± 0.09	0.0	−2.26 ± 0.09
Fe_2O_3	42.13 ± 0.28	9.09 ± 3.49	−2.53 ± 0.09
FeO	13.65 ± 0.15	2.92 ± 1.62	−0.45 ± 0.03
MgO	11.69 ± .08	3.27 ± 0.17	0.27 ± 0.07
CaO	16.53 ± 0.06	3.74 ± 0.12	0.34 ± 0.05
Na_2O	28.88 ± 0.06	7.68 ± 0.10	−2.40 ± 0.05
K_2O	45.07 ± 0.09	12.08 ± 0.20	−6.75 ± 0.14
Li_2O	16.85 ± 0.15	5.25 ± 0.81	−1.02 ± 0.06
H_2O	26.27 ± 0.5	9.46 ± 0.83	−3.15 ± 0.61
CO_2	25.4 ± 1.0	10.86 ± 1	−3.82 ± 0.8

Modified after Lange and Carmichael (1990), Lange (1997), Ochs and Lange (1997), and Ghiorso and Gualda (2014, this volume). Uncertainties are 1σ.

TABLE S5.2 Molar Volume of Typical Silicate Crystals and Melts at High Temperature and 10^{-4} GPa. Depolymerized Compositions Typically Decrease in Density 10–20% upon Fusion. The Volume Change Is Less for Tetrahedral Fluids Such as SiO_2. Molar Volumes at 1400 °C, Except for H_2O at 273 K.

Mineral	Melting Temperature (K)	V_{melt} (10^{-6} m^3/mol)	$V_{crystal}$ (10^{-6} m^3/mol)	V_m/V_c	ΔV_{fusion} (10^{-6} m^3/mol)
SiO_2 (cristobalite)	1999	26.91	27.44	0.98	−0.53
$NaAlSi_3O_8$	1393	112.83	104.13	1.08	8.64
$KAlSi_3O_8$	1473	121.24	111.72	1.09	9.75
$CaAl_2Si_2O_8$	1830	108.41	103.42	1.05	5.48
$CaSiO_3$	1817	43.89	41.87	1.05	2.31
$MgSiO_3$	1830	38.85	33.07	1.18	5.99
$CaMgSi_2O_6$	1665	81.80	69.74	1.18	12.62
$Ca_2MgSi_2O_7$	1727	99.70	97.10	1.03	2.60
$Ca_3MgSi_2O_8$	1848	118.09	105.92	1.12	13.07
Fe_2SiO_4	1490	53.15	48.29	1.11	5.49
Mg_2SiO_4	2174	52.37	47.41	1.12	5.53
$CaTiSiO_5$	1670	67.61	57.57	1.17	10.04
H_2O (ice)	273	18.01	19.64	0.92	1.63

Modified from Lange and Carmichael (1990).

TABLE S5.3 Density and Viscosity of Molten Carbonate (Jones et al., 1995 and Sykes et al., 1992) and Supercritical H_2O (Haar et al., 1984).

Composition	Pressure (GPa)	Temperature (°C)	Density (kg/m^3)	Viscosity (Pa s)
$K_2Ca(CO_3)_2$	10^{-4}	975	2014	—
	2.5	950	2750	0.032
	2.5	1150	2580	0.018
	4.0	1050	2800	0.023
K_2CO_3	4	1500	3100	0.023
$K_8Ca_3Mg(CO_3)_8$	2	1250	–	0.065
$K_2Mg(CO_3)_2$	3	800	–	0.036
	3	900	–	0.022
	5.5	1200	–	0.006
H_2O	0.3	500	–	10^{-4}
		800	–	7×10^{-5}

TABLE S5.4 Approximate Values of the Isothermal Bulk Modulus (K_T) and Its Pressure derivative ($K' = dK_T/dP$) for Use in the Birch–Murnaghan Equation of State for Some Simple and Naturally Occurring Silicate Melts at High Temperature (T_o). The Temperature Derivative, dK_T/dT, has Been Constrained Only for a Few Compositions.

Composition	K_T (GPa)	K'	dK_T/dT	T_o (K)	Data Source*
Simple Systems					
$CaMgSi_2O_6$	22.4	6.9	—	1773	(1)
$CaAl_2Si_2O_8$	17.9	5.3	—	1923	(1)
Fe_2SiO_4	19.4	5.3	—	1773	(2)
Naturally Occurring					
Rhyolite (0–8 wt% H_2O)	11.5	6.5	−0.0016	1273	(3)
Andesite (0– 9 wt% H_2O)	17.2	6.3	—	1273	(4)
Basalt (anhydrous)	19.3	4.4	—	1673	(5)
Basalt (anhydrous)	20.8	4.6	—	1673	(6)
Basalt (2 wt% H_2O)	18.2	4	—	2573	(6)
Basalt (8 wt% H_2O)	14.5	3.2		2473	(6)
Komatiite (anhydrous)	26.0	4.3	—	2073	(5)
Komatiite (anhydrous)	23.1	4.9	—	2073	(6)
Peridotite (anhydrous)	23.4	6.2	—	2273	(6)
Peridotite (anhydrous)	24	7.3	−0.0027	2100	(7)
Peridotite (5 wt% H_2O)	8.8	9.9	−0.0022	1773	(8)
Peridotite (~2 wt% CO_2)	23	8.5	−0.01	1800	(9)

**(1) Rigden et al., (1989); (2) Thomas et al., 2012; (3) Malfait et al., 2014a; (4) Malfait et al., 2014b; (5) Agee, 1998; (6) refits by Jing and Karato, 2008, of published sink/float constraints, see additional references therein; (7) Sakamaki et al., 2010; (8) Sakamaki et al., 2009; (9) Sakamaki et al., 2011.*

TABLE S5.5 Melting Temperature, Molar and Specific Enthalpy of Fusion and Entropy of Fusion at 10^{-4} GPa for Some Silicate and Oxide Phases.

Formula	Melting Temperature (K)	ΔH_{fus} (kJ/mole)	ΔS_{fus} (J/mole-K)	Δh_{fus} (kJ/kg)
H_2O	273	7.401	27.11	116
NH_3	195	5.657	29.01	333
CH_4	90.6	0.937	10.34	58
ZrO_2 (baddeleyite)	3123	87.03	27.87 ± 0.02	706
$Fe_{0.947}O$	1652	31.3 ± 0.2	19.0 ± 0.1	454
$FeTiO_3$	1640	21.7 ± 0.1	13.2 ± 0.1	143
TiO_2 (rutile)	1870	67.0 ± 0.1	35.8 ± 0.1	838
Fe_2O_3 (hematite)	1895	114.5 ± 0.2	60.4 ± 0.2	717
PbO (Massicot)	1170	25.52 ± 0.01	21.81	114

(*Continued*)

TABLE S5.5 Melting Temperature, Molar and Specific Enthalpy of Fusion and Entropy of Fusion at 10^{-4} GPa for Some Silicate and Oxide Phases.—Cont'd

Formula	Melting Temperature (K)	ΔH_{fus} (kJ/mole)	ΔS_{fus} (J/mole-K)	Δh_{fus} (kJ/kg)
Fe_3O_4 (Magnetite)	1870	138.07 ± 0.05	73.83	596
$LiAlO_2$	1883	87.9 ± 0.3	46.7 ± 0.5	1333
$MgAlO_2$	2408	107 ± 11	44 ± 4	752
$Ca_2Fe_2O_5$	1750	151.0 ± 0.5	86.3 ± 0.1	556
Al_2O_3	2323	107.5 ± 54	46.3 ± 23	1054
SiO_2 (quartz)[a]	1700	9.40 ± 1.0	5.53 ± 0.56	157
SiO_2 (cristobalite)	1999	8.92 ± 1.0	4.46 ± 0.50	149
$MgSiO_3$[a]	1834	73.2 ± 6.0	39.9 ± 3.3	729
$CaSiO_3$ (wollastonite)[a]	1770	61.7 ± 4.0	34.9 ± 2.3	531
$CaSiO_3$ (pseudowoll)	1817	57.3 ± 2.9	31.5 ± 1.6	493
$CaMgSi_2O_6$	1665[b]	137.7 ± 2.4	82.7 ± 1.4	636
$Ca_2MgSi_2O_7$	1727	123.9 ± 3.2	71.7 ± 1.9	454
$Ca_3MgSi_3O_8$[b]	1848	125 ± 15	67.5 ± 8.1	350
Fe_2SiO_4	1490[a]	89.3 ± 1.1	59.9 ± 0.7	438
Mn_2SiO_4	1620	89.0 ± 0.5	55.2 ± 0.3	633
Mg_2SiO_4	2174	142 ± 14	65.3 ± 6	1010
$CaTiSiO_5$	1670	123.8 ± 0.4	74.1 ± 0.2	755
$NaAlSi_3O_8$	1393	64.5 ± 3.0	46.3 ± 2.2	246
$NaAlSi_2O_6$[a]	1100	59.3 ± 3.0	53.9 ± 2.7	293
$NaAlSiO_4$[a]	1750	49.0 ± 2.1	28.0 ± 1.2	345
$Na_2Si_2O_5$	1147	35.6 ± 4.1	31.0 ± 3.6	196
$KAlSi_3O_8$[a]	1473	57.7 ± 4.2	39.2 ± 2.8	207
$CaAl_2SiO_8$	1830	133.0 ± 4.0	72.7 ± 2.2	478
$Mg_3Al_2Si_3O_{12}$[a]	1500	243 ± 8	162 ± 5	603
$Mg_2Al_4Si_5O_{18}$[a]	1740	346 ± 10	199 ± 6	591
$KMg_3AlSi_3O_{10}F_2$	1670	308.8 ± 1.3	185 ± 1	733

[a] *Metastable congruent melting.*
[b] *Incongruent melting.*
Data compiled from Kelly (1936), Robie and Hemingway (1995), Ghiorso (2004) and references therein.

TABLE S5.6 Coefficients for Estimating the Isobaric Heat Capacity of Silicate Glasses Valid for Temperatures in the Range 400 K < T < 1000 K at 10^{-4} GPa. X_i Is the Mole Fraction of the ith Oxide Component. The gfw Is Defined According to gfw = $\sum X_i M_i$, Where M_i is the Molar Mass of the ith Component.

$$C_p(T) = \sum a_i X_i + \sum b_i X_i T + \sum c_i X_i T^{-2} \left(J K^{-1} gfw^{-1}\right)$$

	a_i	$b_i \times 10^2$	$c_i \times 10^{-5}$
SiO_2	66.354	0.7797	−28.003
TiO_2	33.851	6.4572	4.470
Al_2O_3	91.404	4.4940	−21.465
Fe_2O_3	58.714	11.3841	19.915
FeO	40.949	2.9349	−7.6986
MgO	32.244	2.7288	1.7549
CaO	46.677	0.3565	−1.9322
Na_2O	69.067	1.8603	2.9101
K_2O	107.194	−3.2194	−28.929

Modified after Stebbins et al. (1984).

TABLE S5.7 Partial Molar Isobaric Heat Capacity for Molten Oxide Components Applicable to Silicate Melts at 10^{-4}GPa. C_p is Approximately Independent of Temperature at T ≥ 1400 K.

$$C_p = \sum C_{pi} X_i \left(J K^{-1} gfw^{-1}\right)$$

	Molar C_{pi} (J/gfw K)	Specific c_{pi} (J/kg K)
SiO_2	80.0 ± 0.9	1331
TiO_2	111.8 ± 5.1	1392
Al_2O_3	157.6 ± 3.4	1545
Fe_2O_3	229.0 ± 18.4	1434
FeO	78.9 ± 4.9	1100
MgO	99.7 ± 7.3	2424
CaO	99.9 ± 7.2	1781
SrO	88.7 ± 8	855
BaO	83.4 ± 6.0	544
H_2O molecular	41 ± 14.0	2278
$(OH)^-$ hydroxyl	153 ± 18	8500
Li_2O	104.8 ± 3.2	3507
Na_2O	102.3 ± 1.9	1651
K_2O	97.0 ± 5.1	1030
Rb_2O	97.9 ± 3.6	524

Modified from Stebbins et al. (1984). Water values from Bouhifd et al. (2006).

TABLE S5.8 Thermal Conductivity of Some Geosilicate Crystals, Glasses and Melts at 1 bar.

Composition and state	Temperature (°C)	Thermal Conductivity (W/m K)	Data Source*
Olivine (Fo_{90})	800	2.69	(1)
	1400	2.18	(1)
Forsterite	400	2.47	(1)
	800	1.84	(1)
	1400	1.59	(1)
Orthopyroxene (bronzite)	0	4.62	(1)
	300	3.05	(1)
Diopside	20	4.27	(1)
Diabase	300	2.09	(1)
Obsidian (rhyolite glass)	0	1.34	(1)
	300	1.67	(1)
	500	1.89	(1)
Basalt glass	0	1.15	(1)
	300	1.48	(1)
SiO_2 (glass)	600	1.76	(1)
	1230	1.87	(1)
$NaAlSi_3O_8$ (glass)	25	1.37	(2)
	800	1.56	(2)
$CaAl_2Si_2O_8$ (glass)	25	1.13	(2)
	800	1.43	(2)
$CaMgSi_2O_6$ (glass)	25	1.24	(2)
	800	1.46	(2)
$KAlSi_3O_8$ (glass)	25	1.12	(2)
	800	1.44	(2)
SiO_2 (liquid)	1400	1.32	(2)
	1700	1.41	(2)
$CaMgSi_2O_6$ (liquid)	1100	1.21	(3)
$CaAl_2SiO_8$ (liquid)	1200	1.45	(3)
$NaAlSi_3O_8$ (liquid)	1200	1.59	(3)
$KAlSi_3O_8$ (liquid)	1200	1.45	(3)
Rhyolite (liquid)	800–1100	~1.5	(3)

(1) Clark (1966); (2) Hofmeister et al. (2009); (3) Pertermann et al. (2008).

TABLE S5.9 Thermal Conductivity for Geosilicate Liquids at Elevated Pressure Determined by Molecular Dynamics Simulation.

Temperature (°C)	Pressure (GPa)	Thermal Conductivity (W/m K)
$CaMgSi_2O_6$ liquid		
1800	0	1.14
1800	10	2.02
2800	0	1.02
2800	10	1.94
4000	0	0.77
4000	10	1.85
$NaAlSi_3O_8$ liquid		
1800	0	1.45
1800	10	2.16
2800	0	0.99
2800	10	2.55
3750	0	0.89
3750	10	1.89
Mg_2SiO_4 liquid		
3000	0	1.06
3300	0	0.90
3300	6.3	1.83
3300	10	2.11
3800	0	0.89
4300	0	0.68

Data from Tikunoff and Spera (2014).

TABLE S5.10 Activation Energies (E_a) and Preexponential Factors (D_o) for Self/Tracer Diffusivities in Anhydrous Basaltic (46–49.7 wt% SiO_2) Melts. Extreme Caution Should Be Exercised Extrapolating Beyond the Experimental T and P Range.

Species	P (GPa)*	T Range (K)	E_a (kJ/mol)	$\ln D_o$ (D_o in m^2/s)	Data Source#
Li	10^{-4} (a)	1569–1673	116	−11.8	(1)
Na	10^{-4} (a)	1577–1692	164	−9.3	(2)
Cs	10^{-4} (a)	1567–1675	274	−4.4	(2)
Ca	10^{-4} (a)	1538–1723	184	−9.8	(3)
Sr	10^{-4} (a)	1538–1723	182	−10.5	(3)
Sr	10^{-4} (a)	1567–1675	191	−9.7	(2)
Sr	1 (gr)	1528–1738	136	−14.4	(4)

(*Continued*)

TABLE S5.10 Activation Energies (E_a) and Preexponential Factors (D_o) for Self/Tracer Diffusivities in Anhydrous Basaltic (46–49.7 wt% SiO_2) Melts. Extreme Caution Should Be Exercised Extrapolating Beyond the Experimental T and P Range.—Cont'd

Species	P (GPa)*	T Range (K)	E_a (kJ/mol)	$\ln D_o$ (D_o in m^2/s)	Data Source#
Ba	10^{-4} (a)	1538–1723	165	−12.0	(3)
Ba	10^{-4} (a)	1572–1692	170	−11.7	(2)
Sc	10^{-4} (a)	1572–1675	198	−10.3	(2)
Mn	10^{-4} (a)	1567–1671	166	−11.2	(2)
Fe^{+3}	10^{-4} (a)	1570–1675	265	−4.8	(2)
Co	10^{-4} (a)	1567–1671	197	−9.0	(2)
Co	10^{-4} (a)	1538–1723	152	−12.1	(3)
Si	1 (gr)	1593–1873	167	−12.8	(6)
O	10^{-4} (v)	1593–1773	251	−6.6	(7)
O	1 (gr)	1593–1873	172	−12.4	(6)
Eu^{+3}, Gd	10^{-4} (a)	1593–1713	170	−12.1	(5)
Eu^{+3}	10^{-4} (a)	1567–1673	268	−5.0	(8)
Eu^{+3}	10^{-4} (a)	1577–1672	248	−9.3	(8)

**(a), run in air; (v), run at variable log fO_2 between 0 and −3.3; (gr), enclosed in graphite capsule.*
#(1) Lowry et al., 1981; (2) Lowry et al., 1982; (3) Hofmann and Magaritz, 1977; (4) Lesher, 1994; (5) Magaritz and Hofmann, 1978; (6) Lesher et al., 1996; (7) Canil, 1990; (8) Hendersen et al., 1985.

TABLE S5.11 Activation Energies (E_a) and Preexponential Factors (D_o) for Self/Tracer diffusivities in Anhydrous Rhyolitic (69–76 wt% SiO_2) Melts. Extreme Caution Should Be Exercised Extrapolating Beyond the Experimental T and P Range.

Species	P (GPa)*	T Range (K)	E_a (kJ/mol)	$\ln D_o$ (D_o in m^2/s)	Data Source*
Li	10^{-4} (a)	1573–1673	84	−13.8	(1)
Na	10^{-4} (a)	1573–1673	152	−9.6	(2)
Cs	10^{-4} (a)	1573–1673	219	−10.7	(2)
Cs	10^{-4} (a)	1063–1573	201	−13.8	(3)
Ca	10^{-4} (a)	903–1203	284	−1.6	(3)
Ba	10^{-4} (a)	1573–1673	130	−16.6	(2)
Ba	10^{-4} (a)	1433–1588	199	−11.2	(2)
Sr	1 (gr)	1528–1738	136	−16.3	(4)
Mn	10^{-4} (a)	1573–1673	210	−10.6	(2)
Fe^{+3}	10^{-4} (a)	1573–1673	177	−14.4	(2)
Co	10^{-4} (a)	1573–1673	167	−13.9	(2)
B	1 (gr)	1573–1773	400	−1.7	(5)
Ga	1 (gr)	1573–1773	347	−4.3	(5)
Si	1 (gr)	1573–1773	139	−23.0	

TABLE S5.11 Activation Energies (E_a) and Preexponential Factors (D_o) for Self/Tracer diffusivities in Anhydrous Rhyolitic (69–76 wt% SiO_2) Melts. Extreme Caution Should Be Exercised Extrapolating Beyond the Experimental T and P Range.—Cont'd

Species	P (GPa)*	T Range (K)	E_a (kJ/mol)	$\ln D_o$ (D_o in m^2/s)	Data Source*
Si	1 (gr)	1733–1935	380	−3.8	(6)
Si	2 (gr)	1733–1935	305	−8.3	(6)
Si	4 (gr)	1733–1935	163	−15.9	(6)
O	1 (gr)	1733–1935	293	−8.9	(6)
O	2 (gr)	1733–1935	264	−10.2	(6)
O	4 (gr)	1733–1935	155	−15.9	(6)
Eu^{+3}	10^{-4} (a)	1473–1673	253	−9.0	(2)
Eu^{+3}	10^{-4} (a)	973–1323	289	−7.2	(3)
Ce	10^{-4} (a)	1148–1373	490	6.3	(3)
Nd	1 (gr)	1528–1738	198	−13.7	(4)
U^{+6}	10^{-4} (a)	1250–1923	364	−6.7	(7)
Th	10^{-4} (a)	1250–1923	369	−7.0	(7)

(a), run in air; (gr), enclosed in graphite capsule.
(1) Cunningham et al., 1983; (2) Hendersen et al., 1985; (3) Jambon, 1982; (4) Lesher, 1994; (5) Baker, 1992; (6) Tinker et al., 2001; (7) Mungall, 1997.

ACKNOWLEDGMENTS

This material is based upon work supported by the National Science Foundation under grants EAR-1019887 and EAR-1215714, and the U.S. Department of Energy under contract DE-FG-03-91ER-14211. This research also used resources of the National Energy Research Scientific Computing Center (NERSC) supported by U.S. Department of Energy contract DE-AC02-05CH11231. CEL acknowledges support from the Danish National Research Foundation for the Niels Bohr Professorship at Aarhus University during production of this chapter. Any opinions, findings, and conclusions or recommendations expressed in this chapter are those of the authors and do not necessarily reflect the views of agencies funding this work.

FURTHER READING

Agee, C.B., 1998. Crystal-liquid density inversions in terrestrial and lunar magmas. Phys. Earth Planet. Int 107, 63–74.

Baker, D.R., 1992. Tracer diffusion of network formers and multicomponent diffusion in dacitic and rhyolitic melts. Geochim Cosmochim Acta 56 (2), 617–631.

Bouhifd, M., Whittington, A., Roux, J., Richet, P., 2006. Effect of water on the heat capacity of polymerized aluminosilicate glasses and melts. Geochimica et Cosmochimica Acta 70, 711–722.

Brouwers, H.J.H., 2010. Viscosity of a concentrated suspension of rigid monosized particles. Physical Review E 81, 051402.

Canil, D., Muehlenbachs, K., 1990. Oxygen diffusion in a Fe-rich basalt melt. Geochim Cosmochim Acta 54, 2947–2951.

Clark Jr, S.P., 1966. Thermal conductivity. GSA Memoirs 97, 459–482.

Cunningham, G.J., Henderson, P., Lowry, R.K., Nolan, J., Reed, S.J.B., Long, J.V.P., 1983. Lithium diffusion in silicate melts. Earth Planet Sci Lett 65, 203–205.

Dingwell, D.B., Webb, S.L., 1989. Structural relaxation in silicate melts and non-Newtonian melt rheology in geologic processes. Physics and Chemistry of Minerals 16, 508–516.

Dobson, D.P., Jones, A.P., Rabe, R., Sekine, T., Kurita, K., Taniguchi, T., Kondo, T., Kato, T., Shimomura, O., Urakawa, S., 1996. In-situ measurement of viscosity and density of carbonate melts at high pressure. Earth Planet. Sci. Lett 143, 207–215.

Ghiorso, M.S., 2004. An equation of state for silicate melts. III. Analysis of shock compression data and mineral fusion curves. Am. J. Sci 304, 752–810.

Ghiorso, M., Gualda, G., 2015. Chemical Thermodynamics and the Study of Magmas. In: Sigurdsson, H., Houghton, B.F., McNutt, S.R., Rymer, H., Stix, J. (Eds.), Encyclopedia of Volcanoes. Elsevier, pp. 143–161.

Giordano, D., Russell, J.K., Dingwell, D.B., 2008. Viscosity of magmatic liquids: a model. Earth and Planetary Science Letters 271, 123–134.

Haar, L., Gallagher, J., Kell, G., 1984. NBS/NRC Steam Tables: Thermodynamic and Transport Properties and Computer Programs for Vapor and Liquid States of Water in SI Units. Hemisphere Publishing Corporation, Washington, 320 pp.

Henderson, P., Nolan, J., Cunningham, G.C., Lowry, R.K., 1985. Structural controls and mechanisms of diffusion in natural silicate melts. Contrib Mineral Petrol 89, 263–272.

Hofmann, A.W., Magaritz, M., 1977. Diffusion of Ca, Sr, Ba, and Co in a basalt melt - implications for geochemistry of mantle. J Geophy Res 82, 5432−5440.

Hofmeister, A.M., Whittington, A.G., Pertermann, M., 2009. Transport properties of high albite crystals and near-endmember feldspar and pyroxene glasses and melts to high temperature. Contrib. Mineral. Petrol 158, 381−400.

Jambon, A., 1982. Tracer diffusion in granitic melts - Experimental results for Na, K, Rb, Cs, Ca, Sr, Ba, Ce, Eu to 1300 Degrees C and a model of calculation. J Geophy Res 87, 797−810.

Jing, Z., Karato, S., 2008. Compositional effect on the pressure derivatives of bulk modulus of silicate melts. Earth Planet Sci Lett 272, 429−436.

Jones, A.P., Dobson, D., Genge, M., 1995. Comment on physical properties of carbonatite magmas inferred from molten salt data, and application to extraction patterns from carbonatite-silicate magma chambers. Geol. Mag 132, 121−121.

Kelley, K.K., 1936. Contributions to data on theoretical metallurgy: V. Heats of fusion of inorganic compounds. U.S. Bur. Mines Bull 393, 166.

Lange, R.A., Carmichael, I.S.E., 1990. Thermodynamic properties of silicate liquids with emphasis on density, thermal expansion and compressibility. Reviews in Mineral 24, 25−59.

Lange, R.A., 1997. A revised model for the density and thermal expansivity of K_2O-Na_2O-CaO-MgO-Al_2O_3-SiO_2 liquids from 700 to 1900 K: extension to crustal magmatic temperatures. Contrib. Mineral. Petrol 130, 1−11.

Lesher, C.E., 2010. Self-diffusion in silicate melts: theory, observations and applications to magmatic systems. Reviews in Mineralogy and Geochemistry 72, 269−309.

Lesher, C.E., Hervig, R.L., Tinker, D., 1996. Self diffusion of network formers (silicon and oxygen) in naturally occurring basaltic liquid. Geochim Cosmochim Acta 60, 405−413.

Lowry, R.K., Henderson, P., Nolan, J., 1982. Tracer diffusion of some alkali, alkaline-earth and transition element ions in a basaltic and an andesitic melt, and the implications concerning melt structure. Contrib Mineral Petrol 80, 254−261.

Lowry, R.K., Reed, S.J.B., Nolan, J., Henderson, P., Long, J.V.P., 1981. Lithium tracer-diffusion in an alkali-basaltic melt - an ion-microprobe determination. Earth Planet Sci Lett 53, 36−40.

Magaritz, M., Hofmann, A.W., 1978. Diffusion of Sr, Ba and Na in obsidian. Geochim. Cosmochim. Acta 42, 595−605.

Malfait, W.J., Seifert, R., Petitgirard, S., Mezouar, M., Sanchez-Valle, C., 2014b. The density of andesitic melts and the compressibility of dissolved water in silicate melts at crustal and upper mantle conditions. Earth Planet Sci Lett 393, 31−38.

Malfait, W.J., Seifert, R., Petitgirard, S., Perrillat, J.-P., Mezouar, M., Ota, T., Nakamura, E., Lerch, P., Sanchez-Valle, C., 2014a. Supervolcano eruptions driven by melt buoyancy in large silicic magma chambers. Nature Geoscience 7, 122−125.

Mungall, J.E., Dingwell, D.B., 1997. Actinide diffusion in a haplogranitic melt: Effects of temperature, water content and pressure. Geochim Cosmochim Acta 61, 2237−2246.

Mungall, J.E., 2002. Empirical models relating viscosity and tracer diffusion in magmatic silicate melts. Geochimica et Cosmochimica Acta 66, 125−143.

Mysen, B.O., Richet, P., 2005. Silicate Glasses and Melts. Elsevier, New York.

Navrotsky, A., 1995. Energetics of silicate melts. Reviews in Mineral 32, 121−149.

Nevins, D., Spera, F.J., 1998. Molecular dynamics simulations of molten $CaAl_2Si_2O_8$: Dependence of structure and properties on pressure. Am Mineral 83, 1220−1230.

Ochs III, F.A., Lange, R.A., 1997. The partial molar volume, thermal expansivity, and compressibility of H_2O in $NaAlSi_3O_8$ liquid: new measurements and an internally consistent model. Contrib Mineral Petrol 129, 155−165.

Pertermann, M., Whittington, A.G., Hofmeister, A.M., Spera, F., Zayak, J., 2008. Transport properties of low-sanidine single-crystals, glasses and melts at high temperature. Contrib Mineral Petrol 155, 689−702.

Richet, P., 1983. Viscosity and configurational entropy of silicate melts. Geochim Cosmochim Acta 48, 471−483.

Richet, P., Bottinga, Y., 1995. Rheology and configurational entropy of silicate melts. Rev.. in Mineral 32, 67−89.

Rigden, S.M., Ahrens, T.J., Stolper, E.M., 1989. High-pressure equation of state of molten anorthite and diopside. J. Geophys. Res 94, 9508−9522.

Rivers, M.L., Carmichael, L.S.E., 1987. Ultrasonic studies of silicate melts. Jour. Geophys. Res 92, 9247−9270.

Robie, R.A., Hemingway, B.S., 1995. Thermodynamic properties of minerals and related substances at 298.15 K and 1 bar (10^5 pascals) pressure and at higher temperatures. USGS Bulletin 2131.

Sakamaki, T., Ohtani, E., Urakawa, S., Hidenori Terasaki, H., Katayama, Y., 2011. Density of carbonated peridotite magma at high pressure using an X-ray absorption method. Am. Mineral 96, 553−557.

Sakamaki, T., Ohtani, E., Urakawa, S., Suzuki, A., Katayama, Y., 2009. Measurement of hydrous peridotite magma density at high pressure using the X-ray absorption method. Earth Planet Sci Lett 287, 293−297.

Sakamaki, T., Ohtani, E., Urakawa, S., Suzuki, A., Katayama, Y., 2010. Density of dry peridotite magma at high pressure using an X-ray absorption method. Am. Mineral 95, 144−147.

Scarfe, C.M., Mysen, B.O., Virgo, D., 1987. Pressure dependence of the viscosity of silicate melts. In: Mysen, B.O. (Ed.), Magmatic Processes: Physicochemical Principles, Geochem. Sec, 1, pp. 59−67. Special Publication.

Shaw, H.R., 1972. Viscosities of magmatic silicate liquids: an empirical method of prediction. American Journal of Science 272, 870−893.

Spera, F.J., Ghiorso, M., Nevins, D., 2011. Structure, thermodynamic and transport properties of liquid $MgSiO_3$: comparison of molecular models and laboratory results. Contributions to Mineralogy and Petrology 75, 1272−1296.

Stebbins, J.F., Carmichael, I.S.E., Moret, L.K., 1984. Heat capacities and entropies of silicate liquids and glasses. Contrib Mineral Petrol 86, 131−148.

Stixrude, L., Lithgow-Bertelloni, C., 2010. Thermodynamics of the earth's mantle. In: Wentzcovitch, R., Stixrude, L. (Eds.), Theoretical and Computational Methods in Mineral Physics, Reviews in Mineral and Geochemistry, 71, pp. 465−484.

Sykes, D., Baker, M.B., Wyllie, P.J., 1992. Viscous properties of carbonate melts at high pressure, EOS. Trans. Am. Geophy. Union 73, 372.

Thomas, C.W., Liu, Q., Agee, C.B., Asimow, P.D., Lange, R.A., 2012. Multi-technique equation of state for Fe_2SiO_4 melt and the density of Fe-bearing silicate melts from 0 to 161 GPa. J. Geophys. Res 117, B10206.

Tikunoff, D., Spera, F.J. Thermal conductivity of molten and glassy $NaAlSi_3O_8$, $CaMgSi_2O_6$ and Mg_2SiO_4 by non equilibrium molecular dynamics at elevated temperature and pressure: part 1 – methods and results. American Mineralogist, 99(11–12), pp. 2328–2336.

Tinker, D., Lesher, C.E., 2001. Self diffusion of Si and O in dacitic liquid at high pressures. Am Mineral 86, 1–13.

Urbain, G., Bottinga, Y., Richet, P., 1982. Viscosity of liquid silica, silicates and alumino-silicates. Geochimica et Cosmochimica Acta 46, 1061–1072.

Zarzycki, J., 1991. In: Chan, R.W. (Ed.), Glasses and the Vitreous State. Cambridge University Press, Cambridge, pp. 505.

Zhang, Y., Ni, H., Chen, Y., 2010. Diffusion data in silicate melts. Reviews in Mineralogy and Geochemistry 72, 311–408.